Journal of Physical and Chemical Reference Data

W2020: A Database of Validated Rovibrational Experimental Transitions and Empirical Energy Levels of $H_2{}^{16}O$

Cite as: J. Phys. Chem. Ref. Data **49**, 033101 (2020); https://doi.org/10.1063/5.0008253
Submitted: 19 March 2020 . Accepted: 26 May 2020 . Published Online: 01 July 2020

Tibor Furtenbacher, Roland Tóbiás, Jonathan Tennyson, Oleg L. Polyansky, and Attila G. Császár

Journal of Physical and Chemical Reference Data ARTICLE scitation.org/journal/jpr

W2020: A Database of Validated Rovibrational Experimental Transitions and Empirical Energy Levels of $H_2{}^{16}O$

Cite as: J. Phys. Chem. Ref. Data 49, 033101 (2020); doi: 10.1063/5.0008253
Submitted: 19 March 2020 • Accepted: 26 May 2020 •
Published Online: 1 July 2020

View Online Export Citation CrossMark

Tibor Furtenbacher,[1] Roland Tóbiás,[1] Jonathan Tennyson,[2] Oleg L. Polyansky,[2] and Attila G. Császár[3,a)]

AFFILIATIONS

[1]MTA-ELTE Complex Chemical Systems Research Group, P.O. Box 32, H-1518 Budapest 112, Hungary
[2]Department of Physics and Astronomy, University College London, Gower Street, London WC1E 6BT, United Kingdom
[3]Institute of Chemistry, ELTE Eötvös Loránd University, Pázmány sétány 1/A, H-1117 Budapest, Hungary and MTA-ELTE Complex Chemical Systems Research Group, P.O. Box 32, H-1518 Budapest 112, Hungary

[a)]**Author to whom correspondence should be addressed:** csaszarag@caesar.elte.hu

ABSTRACT

A detailed understanding of the complex rotation–vibration spectrum of the water molecule is vital for many areas of scientific and human activity, and thus, it is well studied in a number of spectral regions. To enhance our perception of the spectrum of the parent water isotopologue, $H_2{}^{16}O$, a dataset of 270 745 non-redundant measured transitions is assembled, analyzed, and validated, yielding 19 204 rovibrational energy levels with statistically reliable uncertainties. The present study extends considerably an analysis of the rovibrational spectrum of $H_2{}^{16}O$, published in 2013, by employing an improved methodology, considering about one-third more new observations (often with greatly decreased uncertainties), and using a highly accurate first-principles energy list for validation purposes. The database of experimental rovibrational transitions and empirical energy levels of $H_2{}^{16}O$ created during this study is called W2020. Some of the new transitions in W2020 allow the improved treatment of many parts of the dataset, especially considering the uncertainties of the experimental line positions and the empirical energy values. The W2020 dataset is examined to assess where measurements are still lacking even for this most thoroughly studied isotopologue of water, and to provide definitive energies for the lower and upper states of many yet-to-be-measured transitions. The W2020 dataset allows the evaluation of several previous compilations of spectroscopic data of water and the accuracy of previous effective Hamiltonian fits.

Key words: MARVEL; water vapor; high-resolution spectroscopy; energy levels; rotational-vibrational transitions; atmospheric physics.

CONTENTS

List of Tables

List of Figures

1. Introduction

Several hundred papers exist, spanning almost 100 years of studies, which report laboratory measurements of gas-phase rovibrational transitions within the ground electronic state of water isotopologues. Many of the relevant data have been cited and evaluated in Refs. 1–5, detailing the work of an International Union of Pure and Applied Chemistry (IUPAC) Task Group (TG) on "A Database of Water Transitions from Experiment and Theory" (Project No. 2004-035-1-100). This TG carefully analyzed all the measured and assigned transitions available to them and recommended a large number of validated experimental transitions and the corresponding empirical energy levels for nine major isotopologues of water.[5] The study on the main water isotopologue, $H_2{}^{16}O$,[3] was published in 2013. Since then, a lot of new developments have been made concerning water spectroscopy,[6–44] which impelled us to revisit the task of validating and analyzing an enlarged set of experimental transitions and empirical energy levels of $H_2{}^{16}O$. Furthermore, despite the extensive list of sources considered in Ref. 3, hereafter called Part III (of the IUPAC TG's efforts), a number of spectroscopic studies prior to 2013 have come to our attention, which were not dealt with explicitly during the Part III study.[45–83] Note that the TG's work was built on a previous comprehensive compilation of empirical energy levels of $H_2{}^{16}O$.[84]

Empirical rovibrational energy values of water isotopologues, which can be obtained from the experimental line positions, for example, via the MARVEL (Measured Active Rotational–Vibrational Energy Levels) methodology,[85–87] employed, in fact, during this study, have a number of important applications. The energy levels have been used to supplement, and often replace, the observed transition wavenumbers in spectroscopic databases designed for applications to room-temperature[88–91] and hot[31,92] planetary atmospheres. The availability of accurate energies allows the computation of highly accurate ideal-gas partition functions and related thermodynamic quantities,[93–95] provide input for spectral assignments,[27,32,44] facilitate the testing and construction of revised potential energy surfaces (PESs),[96–99] and expedite the validation of theoretical models, in general.[100] There are also more specific applications, such as the search for *ortho–para* transitions for the $H_2{}^{16}O$ molecule[101] and a reliable prediction for transition frequencies of various water isotopologues.[92] Finally, we mention that limited updates to the Part III data were published as part of our ongoing attempts to improve certain aspects of the MARVEL algorithm.[86,87,102]

This study, dedicated to the high-resolution spectroscopy of the parent water isotopologue, $H_2{}^{16}O$, provides the first major extension of the Part III[3] results. Based on the list of experimental $H_2{}^{16}O$ lines available from the literature, here we present new recommendations for old energy levels, as well as a number of new rovibrational states, by assembling a significantly updated line-by-line spectroscopic database for $H_2{}^{16}O$. Due to the large number of technical developments during the MARVEL analysis and the much enlarged experimental dataset employed, it is suggested that the database collated during this study, called W2020, should replace the list reported earlier by the IUPAC TG (Part III) and should be used exclusively by practitioners of water spectroscopy and those who need rovibrational transitions and energy levels of $H_2{}^{16}O$. In particular, it is expected that the new and improved data of this study will enter the next edition of the canonical spectroscopic database, HITRAN.[88]

2. Methods

2.1. Spectroscopic networks

To obtain the best possible estimates for the rovibrational energy values of $H_2{}^{16}O$, all of the observed high-resolution rovibrational lines taken from the literature were processed simultaneously, yielding a spectroscopic network (SN).[85,103,104] SNs consist of nodes (energy levels) linked by edges (measured or computed transitions), which are oriented from their lower energy levels to their upper ones (independently of whether they were recorded by absorption, emission, or action spectroscopy). Since often there are repeated observations for the same transition, these multiple measurements are represented with multiple edges in the SN. The lines sharing the same upper and lower states form coincidence classes.

The energy levels of SNs often form distinct components, that is, sets not connected by spectral lines. If a component of the SN contains the lowest-energy state of a nuclear-spin isomer of the molecule examined, this component is called a principal component (PC); otherwise, it is a floating component (FC). Excluded energy levels,[87] forming isolated nodes (whose transitions have all been deleted), are all special FCs of the SN. For $H_2{}^{16}O$, no transitions linking energy levels of its two (*ortho* and *para*) nuclear-spin isomers have been observed;[101] thus, the energy separation of the *ortho* and *para* PCs is not known experimentally, though it can be estimated with considerable accuracy.[44]

As dictated by their edge distributions,[104,105] experimental SNs are characterized by a small number of hubs, energy levels incident to a large number of transitions. These hubs are the lower states of a huge number of spectral lines. For further details about the important

network-theoretical notions mentioned, see Ref. 104 and Sec. 2.1 of Ref. 87.

2.2. extMARVEL

During the present study, the extended MARVEL[85–87] scheme (extMARVEL)[87] and the implementation of its automated part (intMARVEL) were utilized to determine accurate empirical energy values for $H_2{}^{16}O$ with well-defined uncertainties from the collated set of observed and assigned rovibrational transitions with specified uncertainties. As shown in Ref. 87, the use of the intMARVEL code helps to retain the high accuracy of the best measurements for the derived energy levels. Since this feature was not available during the Part III compilation and analysis,[3] the W2020 dataset constructed with the extMARVEL protocol exhibits much improved energy values (with more dependable uncertainties), especially for the low-lying rovibrational states of $H_2{}^{16}O$. In the interest of space, only the four most relevant characteristics of the extMARVEL procedure are outlined here; for all the other terms and technical aspects, the reader is referred to Ref. 87.

First, in contrast to the standard MARVEL algorithm, the extMARVEL protocol is based on the use of segments (sets of transitions coming from the same data source with approximately the same experimental uncertainties). For each segment, an estimated segment uncertainty (ESU) is given; its refined value, provided by an analysis of the cycles[106] in the SN, serves as an initial uncertainty value for the lines of this segment. Although line-by-line input uncertainties are not required, originally published uncertainties, if accessible, are still utilized by the intMARVEL code. Second, inversion and the weighted least-squares refinement of the line uncertainties are built upon consecutive addition of transition blocks of decreasing accuracy, leading to highly accurate empirical energy values. The extMARVEL-predicted wavenumbers determined in a particular block are not permitted to be changed by the inclusion of less accurate observations. Third, automatic recalibration of the ill-calibrated segments is performed. As demonstrated earlier,[3] MARVEL is well suited to complete this important task. Fourth, synchronization[87] of the combination difference relations is executed to reduce the uncertainties of the empirical energies.

In Ref. 107, the original six-grade classification scheme[87] of the extMARVEL approach was simplified. Here, we make again a slight change to MARVEL's classification scheme: energy levels are now associated with four so-called resistance labels—R+, strongly resistant; R–, weakly resistant; S, semi-resistant; and U, unresistant. Resistance labels reflect the empirical energy level's reliability, which is an extra, qualitative information beyond that offered by uncertainties, and their resistance toward changes forced upon them by some (at present, less precise) spectral lines. Energy values with the resistance label R+ are deemed to be fully reliable, and the availability of new transitions is not expected to influence them outside of their present uncertainty limits. The other transitions may vary when further, even more accurate transitions will be added to the transition database. Although it is likely that even the non-R+ rovibrational states (particularly those with R– classification) have reliable energy values, they are not fully certified by the extMARVEL analysis. We emphasize again that the uncertainties of the extMARVEL empirical rovibrational energy levels and their resistance labels provide complementary information about the reliability of the levels.

2.3. XML-based management of the transition database

For the traditional MARVEL code,[85,86] the input transitions have to be provided in the form of a plain text file. If each column of the text file consists of the same type of data, this input representation is a reasonable choice for storing the spectral lines processed by MARVEL. However, when different kinds of information (e.g., measured line positions with various units, comments on the transition entries, or some characteristics of the data sources and their segments[87] having approximately the same experimental accuracy) are collected in the same column, a simple text file becomes unsuitable for handling the complex data structure. To support the annotation and the transparent administration of the collated MARVEL transitions, we decided to replace the original input format with a file structure following the rules of the eXtensible Markup Language (XML). An XML-based input helps to (a) maintain provenance of the data; (b) have a timestamp on the individual transitions, reflecting their occasional relabeling; and (c) give a description of the "original" literature information. The XML-based extMARVEL protocol is called xMARVEL. This novel feature of the present study is reflected in the related entries of the supplementary material.

The general structure of MARVEL XML is defined in Fig. 1. Briefly, the root element of MARVEL XML is named *MARVEL*, which contains the *source* elements. A *source* element comprises information about a particular data source [tag name and reference—the latter corresponds to the digital object identifier (DOI) for journal articles]. Each *source* element must include at least one *segment* element, storing data of the related data-source segment. The children of the *segment* element are the input transitions collected in the *line* elements. A *line* element should consist of the following entries: line position (in element *pos*) and its uncertainty (in element *unc*), labels of the upper and lower states (in element *us* and *ls*, respectively), and a unique tag for the identification of the underlying transition entry. A much more detailed discussion of the MARVEL XML format will be given in an upcoming paper.[108]

3. Construction of the W2020 Database

As mentioned in the Introduction, the Part III database[3] of transitions and energy levels served as the starting point of the present xMARVEL study of the rovibrational spectrum of $H_2{}^{16}O$. Extension and improvement of the Part III dataset includes five major, to some extent interrelated, tasks: (a) based on a careful search of the literature, construct the most complete catalog of published experimental lines; (b) set the best possible (often unreported) initial uncertainties for the observed line positions and segment[87] the data sources appropriately to help the uncertainty refinement process; (c) certify the existence of the empirical energy levels by a comparison with their first-principles counterparts (most important here is the PoKaZaTeL[31] list); (d) relying on the xMARVEL energy values, the related assignments, and reliable first-principles results,[31,109] expand the transition database with certain unmeasured, unreported, or even artificial transitions, inspired by well-founded spectroscopic information, and derive further energy levels; and (e) create the best possible, self-consistent labels for the rovibrational states.

As to task (a), the initial, Part III-based dataset was (i) reduced since two of the 98 sources were removed (81Kyro[110] contains only redundant lines, while the transitions of 05ZoShPoTe[111] proved to be not accurate enough to combine them with high-resolution data of

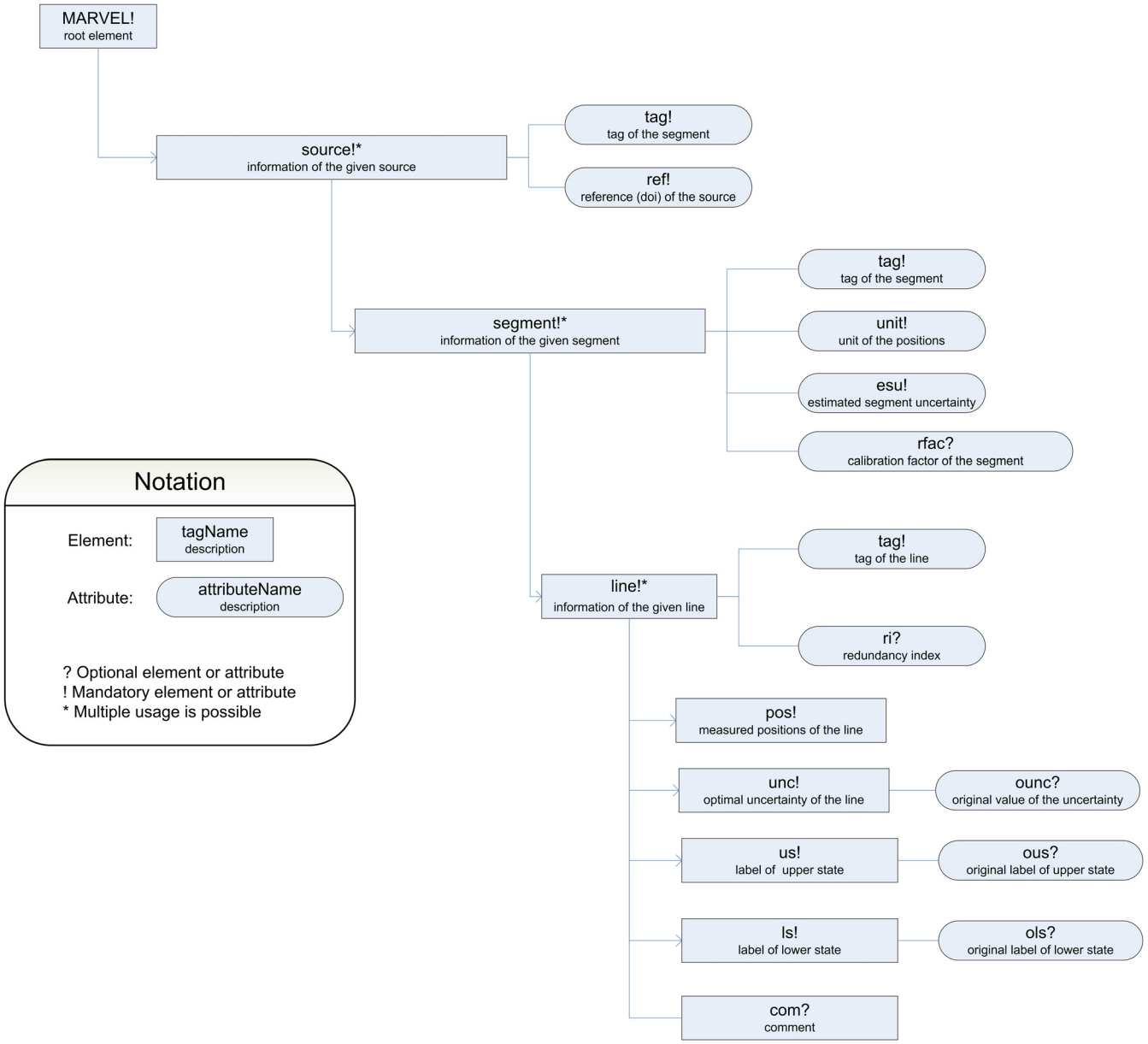

FIG. 1. Definition of MARVEL XML.

other sources), (ii) extended with data sources published after the Part III article, and (iii) enlarged with earlier sources not treated explicitly in Part III. It should also be noted that sources where some lost transitions or lines of unidentified origin were recognized were re-entered afresh into the W2020 database. As a result, 78 new data sources were included in the W2020 database, leading to 174 experimental sources in total.

Concerning task (b), the initial line uncertainties, indispensable for the successful execution of the xMARVEL method, were selected with great care. This is an especially important step as these values determine in which transition block the individual lines should be refined. Thus, all the data sources were divided into segments, and these segments were supplied with estimated segment uncertainties. The ESU values serve as educated guesses for the initial uncertainties of the line positions, except for those transitions, mainly microwave and terahertz, characterized by originally reported individual uncertainties. For the accuracy of particular segments, we tried to adopt the smallest reasonable ESU values to facilitate the generation of correct uncertainty estimates for the derived empirical energies. Accordingly, some segments ended up with higher accuracy than those given in Part III. For example, the expected uncertainties of the segments 06MaToNaMo,[112] 85BrTo,[113] 05Toth,[114] and 99Toth[115]

were modified as follows: $3 \times 10^{-4} \rightarrow 3 \times 10^{-6}$, $1 \times 10^{-3} \rightarrow 1 \times 10^{-4}$, $1 \times 10^{-3} \rightarrow 2 \times 10^{-4}$, and $1 \times 10^{-3} \rightarrow 3 \times 10^{-4}$ (all values in cm^{-1}), respectively. In other cases, slightly larger uncertainties had to be assigned to certain segments for which a systematic increase occurred in the unsigned least-squares residuals (differences between the observed and calculated wavenumbers). An example is 08ZoShOvPo,[116] for which a change (in cm^{-1}) of $5 \times 10^{-3} \rightarrow 2 \times 10^{-2}$ was made to improve the overall consistency of the transition database. Clearly, many of the ESU values are optimized for the W2020 dataset; thus, some of them might need to be modified when future measurements become available.

After the generation of the rovibrational empirical energies, an automated check [task (c)] was performed to certify that they have unique counterparts in the PoKaZaTeL list (based just on J and parity information; see Table 1 of Ref. 3), within a tolerance of $10^{-4} \times E$, where E is the energy of the xMARVEL energy level examined and J is the rotational quantum number. For $E \leq 30\,000$ cm^{-1}, those empirical rovibrational states that could not be matched within this tolerance were excluded from the database, together with the corresponding transitions. Due to these exclusions and some missing links, 148 energy levels became part of FCs. Above 30 000 cm^{-1}, all the energy levels were left intact because, in this region, the PoKaZaTeL PES needs further refinement to ensure that it can be properly utilized for this validation task.

During the execution of task (d), several explicitly unmeasured (and unmeasurable) transitions were placed into the W2020 database. First, the disconnected *ortho* and *para* states were linked with a forbidden line, $(0\ 0\ 0)1_{0,1} \leftarrow (0\ 0\ 0)0_{0,0}$, for which an extremely accurate, empirical wavenumber value,[44] 23.794 361 22(25) cm^{-1}, was adopted. The rovibrational lines of $H_2{}^{16}O$ are designated hereafter using the standard normal-mode–rigid-rotor notation $(v_1' v_2' v_3')J'_{K_a',K_c'} \leftarrow (v_1'' v_2'' v_3'')J''_{K_a''K_c''}$, where $'$ and $''$ refer to the upper and lower state of the given transition, respectively, while the $(v_1\ v_2\ v_3)J_{K_a,K_c}$ descriptors represent a rovibrational state. Here, v_1, v_2, and v_3 are standard[117] vibrational quantum numbers for the symmetric stretch, bend, and asymmetric stretch modes of $H_2{}^{16}O$, respectively, while J_{K_a,K_c} are rigid-rotor asymmetric-top quantum numbers.[118] Second, nearby *ortho* and *para* states were searched for the construction of additional lines, in order to maximize the number of empirically known energy levels. These so-called virtual transitions, collected in source "20virt," were obtained from the PoKaZaTeL energy list, together with their wavenumbers. Third, similar to Part III, close-lying *ortho–para* transition doublets were also utilized. If the PoKaZaTeL energy-level set revealed that the (so-called) complementary (usually *para*) transition (separated by not more than 5×10^{-3} cm^{-1} based on first-principles information) is not reported in the data source of an experimental (mainly *ortho*) line with a σ wavenumber, then this complementary transition was added to the source "20compl" with the same σ wavenumber.

After the derivation of reliable empirical energy values, conflicts arising from the use of different labeling schemes were resolved, and a self-consistent set of normal-mode and rigid-rotor quantum numbers was provided for the energy levels [task (e)]. Note that in the local-mode notation, the standard normal-mode v_1, v_2, and v_3 vibrational quantum numbers are replaced by $(nm)^{\pm}v_2$, where n and m are the number of quanta of OH stretch, while v_2 retains its meaning. The $\pm$ sign also serves as a symmetry label, and it is usual not to indicate + for the $n = m$ cases. For sources 08GrMaZoSh[119] and 09GrBoRiMa,[120] where the vibrational states were originally represented with local-mode quantum numbers, one-to-one conversion (see Table I.1 of Ref. 121) to normal-mode notation was applied. In the case of 09GrBoRiMa, where the v_2 values are missing for some of the transitions, $v_2 = 0$ was assumed.[122]

Unfortunately, there are no theoretical techniques that can yield unambiguous labels for high-lying vibrational bands (say, above 11 000 cm^{-1}, the barrier to linearity of water[123–125]). What makes the situation even more complicated is that it is not unusual that the same authors change their labeling scheme between consecutive publications. For example, the rovibrational state at 10 492.2 cm^{-1} was labeled as $(1\ 2\ 0)14_{8,7}$ in 11MiKaWaCa,[76] while in 17MoMiKaBe,[25] this designation was changed to $(2\ 0\ 0)14_{8,7}$. In the end, we decided to accept, whenever possible, the rovibrational labels of the latest source, hoping that in this way we can minimize labeling conflicts with future measurements. As an additional check, the empirical energies were plotted as an approximately quadratic function of K_a [at fixed v_1, v_2, v_3, J, and $(-1)^{v_3+K_a+K_c}$], and these quadratic trends were slightly smoothed, where feasible, by relabeling some rough outlier states. Note that the original labels are included in the MARVEL XML file of the supplementary material. Finally, we have to point out that there are states where we know that the label attached is incorrect, but we were unable to come up with a feasible label. For example, for the states $(3\ 1\ 0)11_{8,4}$ and $(3\ 0\ 1)11_{8,3}$, part of the lines 18TaMiWaLi.900 and 18TaMiWaLi.901,[36] which can be well matched with the PoKaZaTeL data by J and parity, we could not determine the correct labels. While noting the problem in the XML file, we decided not to exclude these "existing" levels from the W2020 dataset.

Table 1 provides a summary of all the data-source segments used during this work, along with some relevant statistical parameters [ESU values, median segment uncertainties (MSUs), and largest segment uncertainties (LSUs)].[87] This table updates Table 2 of Part III[3] for all the common entries. The data sources applied are partitioned into 200 segments, of which 7 had to be recalibrated (see column 7 of Table 1). For all the segments, the ESUs and MSUs are very similar, implying that the initial uncertainties did not change considerably during the xMARVEL refinement. The final transition database includes 270 745 non-redundant lines from 289 070 experimentally assigned transitions among which 267 289 could be validated during this study.

The number of new transitions, with respect to the Part III dataset, cannot be determined in a reliable way due to two significant changes between the Part III and W2020 data. First, a large number of lines were relabeled at the time of compiling the extended dataset of this study. Second, during the revision of the Part III transitions, we often returned to the original assigned lines of the experimental data sources. This change also implies that originally unassigned transitions, labeled during the operation of the IUPAC TG, were removed from the related sources. Nevertheless, to avoid losing energy levels, those lines assigned in Part III and specifying unique rovibrational states were later reinstated in the database as an extra source, "20extra."

4. Results and Discussion

4.1. Updated xMARVEL energy levels

The W2020 dataset includes 19 427 energy levels of which 19 204 relate to the PCs of the underlying SN, while the others are distributed among 117 FCs. Within these FCs, the number of isolated nodes is 91.

TABLE 1. Data source segments of the W2020 dataset and some of their characteristics[a]

Segment tag	Range	*A*/*N*/*V*	ESU	MSU	LSU	Recalib. Factor
69Kukolich[126]	0.741 68–0.741 68	1/1/1	1.67×10^{-9}	1.67×10^{-9}	1.67×10^{-9}	
09CaPuHaGa[127]	10.715–20.704	7/7/7	1.67×10^{-8}	1.67×10^{-8}	2.67×10^{-8}	
71Huiszoon[128]	6.114 6–6.114 6	1/1/1	5.00×10^{-8}	1.10×10^{-7}	1.10×10^{-7}	
95MaKr[56]	18.577–18.577	1/1/1	6.67×10^{-8}	9.69×10^{-8}	9.69×10^{-8}	
20ToFuSiCs[44]	7 012.7–7 350.0	156/156/156	1.10×10^{-7}	1.10×10^{-7}	3.34×10^{-7}	
20ToFuSiCs_S2[44]	23.794–23.794	1/1/1	2.50×10^{-7}	2.50×10^{-7}	2.50×10^{-7}	
06GoMaGuKn[129]	6.114 6–18.577	12/12/12	1.33×10^{-7}	1.33×10^{-7}	1.64×10^{-6}	
05Golubiat[65]	6.114 6–6.114 6	1/1/1	1.67×10^{-7}	4.56×10^{-7}	4.56×10^{-7}	
07KoTrGoPa[130]	10.715–12.682	3/3/3	1.67×10^{-7}	4.62×10^{-7}	1.57×10^{-6}	
13TrKoViPa[131]	12.682–16.294	7/7/6	3.17×10^{-7}	4.81×10^{-7}	5.87×10^{-7}	
18KaStCaDa[29]	7 164.9–7 185.6	8/8/8	4.00×10^{-7}	4.00×10^{-7}	4.00×10^{-7}	
11Koshelev[72]	25.085–25.085	1/1/1	4.67×10^{-7}	4.67×10^{-7}	4.67×10^{-7}	
89BaGoKhHa[132]	6.114 6–6.114 6	1/1/1	5.00×10^{-7}	5.00×10^{-7}	5.00×10^{-7}	
18ChHuTaSu[26]	12 622–12 665	6/6/6	8.00×10^{-7}	8.00×10^{-7}	2.00×10^{-6}	
71StBe[133]	0.741 68–6.114 6	3/3/3	1.00×10^{-6}	2.30×10^{-6}	8.29×10^{-6}	
73BlBrEdKn[134]	357.52–357.52	1/1/1	1.00×10^{-6}	1.00×10^{-6}	1.00×10^{-6}	
83HeMeLu[135]	13.013–32.954	7/7/7	1.00×10^{-6}	1.07×10^{-6}	9.61×10^{-6}	
83MeLuHe[136]	16.797–32.954	5/5/5	1.00×10^{-6}	1.00×10^{-6}	4.94×10^{-6}	
80Kuze[137]	0.400 57–4.002 6	5/5/5	1.33×10^{-6}	3.34×10^{-6}	8.20×10^{-6}	
48GoWeHiSt[138]	0.741 69–0.741 69	1/1/1	1.67×10^{-6}	5.14×10^{-6}	5.14×10^{-6}	
98ChPaEv[139]	88.650–88.650	1/1/1	1.67×10^{-6}	2.46×10^{-6}	2.46×10^{-6}	
87BaAlAlPo[140]	14.199–19.077	6/6/6	1.70×10^{-6}	1.70×10^{-6}	1.70×10^{-6}	
91AmSc[141]	8.253 7–11.835	5/5/5	2.00×10^{-6}	2.00×10^{-6}	2.00×10^{-6}	
97NaLoInNo[142]	118.32–119.07	5/5/5	2.03×10^{-6}	2.03×10^{-6}	4.33×10^{-6}	
95MaOdIwTs[143]	18.577–162.44	139/139/138	2.50×10^{-6}	2.50×10^{-6}	2.15×10^{-5}	
12YuPeDrMa[144]	9.795 6–90.767	221/217/217	2.50×10^{-6}	2.67×10^{-6}	6.99×10^{-5}	
12YuPeDrMa_S2[144]	51.326–694.49	4 288/4 276/4 264	2.00×10^{-3}	3.76×10^{-4}	3.33×10^{-2}	
09CaPuBuTa[145]	36.604–53.444	9/9/9	3.00×10^{-6}	3.00×10^{-6}	4.86×10^{-6}	
06MaToNaMo[112]	28.685–165.31	104/104/104	3.14×10^{-6}	4.32×10^{-6}	2.44×10^{-5}	
83BuFeKaPo[146]	16.797–21.545	5/5/5	3.34×10^{-6}	3.34×10^{-6}	6.67×10^{-6}	
13YuPeDr[10]	17.690–67.209	182/182/182	3.34×10^{-6}	3.34×10^{-6}	3.34×10^{-5}	
91PeAnHeLu[147]	4.657 0–19.804	30/30/30	3.40×10^{-6}	3.40×10^{-6}	2.17×10^{-5}	
72LuHeCoGo[148]	6.114 6–25.085	14/14/14	5.00×10^{-6}	5.00×10^{-6}	5.00×10^{-6}	
95Pearson[149]	4.330 0–17.220	9/9/9	5.00×10^{-6}	5.00×10^{-6}	1.37×10^{-5}	
11DrYuPeGu[70]	82.862–90.843	26/26/25	5.00×10^{-6}	6.67×10^{-6}	1.62×10^{-5}	
00ChPePiMa[150]	28.054–52.511	17/17/17	8.00×10^{-6}	8.00×10^{-6}	1.89×10^{-5}	
79HeJoMc[151]	0.072 049–0.072 049	1/1/1	1.00×10^{-5}	1.00×10^{-5}	1.00×10^{-5}	
79HeJoMc_S2[151]	1 660.5–1 677.2	2/2/2	1.00×10^{-3}	7.74×10^{-4}	7.77×10^{-4}	
20virt	0.000 000–0.000 010	924/924/924	1.00×10^{-5}	1.00×10^{-5}	1.00×10^{-5}	
20virt_S2	0.000 010–0.000 100	353/353/353	1.00×10^{-4}	1.00×10^{-4}	1.00×10^{-4}	
20virt_S3	0.000 100–0.000 999	530/530/530	1.00×10^{-3}	1.00×10^{-3}	1.49×10^{-3}	
20virt_S4	0.001 004–0.009 997	709/709/709	1.00×10^{-2}	1.00×10^{-2}	1.80×10^{-2}	
19VaTrDoKa[42]	6 071.4–6 079.9	21/20/19	1.50×10^{-5}	2.00×10^{-5}	7.30×10^{-4}	
51Jen[152]	0.741 69–0.741 69	1/1/1	2.00×10^{-5}	2.00×10^{-5}	2.00×10^{-5}	
72FlCaVa[153]	0.741 68–25.085	7/7/7	2.00×10^{-5}	1.00×10^{-5}	2.74×10^{-5}	
06JoPaZeCo[154]	1 485.1–1 486.2	2/1/1	2.00×10^{-5}	1.00×10^{-4}	1.00×10^{-4}	
13LuLiWaLi[8]	12 573–12 752	73/73/73	2.00×10^{-5}	2.20×10^{-5}	5.24×10^{-4}	
05HoAnAlPi[155]	212.56–594.95	165/165/163	3.00×10^{-5}	1.62×10^{-5}	7.58×10^{-4}	
87BeKoPoTr[156]	7.761 6–19.850	5/5/5	3.34×10^{-5}	3.34×10^{-5}	4.63×10^{-5}	
70StSt[49]	18.577–18.577	1/1/1	3.40×10^{-5}	6.26×10^{-6}	6.26×10^{-6}	
96Belov[157]	28.054–30.792	5/5/5	3.40×10^{-5}	9.80×10^{-6}	1.59×10^{-5}	
54KiGo[158]	6.114 6–6.114 6	1/1/1	5.00×10^{-5}	4.04×10^{-5}	4.04×10^{-5}	
83Guelachv[159]	1 066.2–2 296.7	1 179/1 178/1 162	5.00×10^{-5}	2.11×10^{-4}	4.86×10^{-3}	0.999 999 843 29

TABLE 1. (*Continued.*)

Segment tag	Range	*A*/*N*/*V*	ESU	MSU	LSU	Recalib. Factor
96BrMa[160]	5 206.3–5 396.5	28/28/28	5.00×10^{-5}	6.05×10^{-5}	2.50×10^{-4}	
18DeGaViRe[28]	3 645.3–3 976.6	315/315/314	5.00×10^{-5}	1.00×10^{-4}	3.24×10^{-3}	
91Toth[161]	1 072.6–2 265.3	739/739/738	6.00×10^{-5}	1.06×10^{-4}	4.84×10^{-3}	
91Toth_S2[161]	1 06 6.2–2 582.6	235/235/235	2.00×10^{-4}	2.34×10^{-4}	3.80×10^{-3}	
91Toth_S3[161]	1 229.4–2 458.2	38/38/38	2.00×10^{-3}	1.01×10^{-3}	2.87×10^{-2}	
97MiTyKeWi[162]	2 507.2–4 402.8	940/932/925	6.00×10^{-5}	3.51×10^{-4}	5.75×10^{-3}	
95PaHo[163]	177.86–519.59	246/246/245	7.00×10^{-5}	8.31×10^{-5}	1.94×10^{-3}	
93Toth[164]	1 316.1–4 260.4	582/582/582	8.00×10^{-5}	9.00×10^{-5}	1.26×10^{-3}	
93Toth_S2[164]	1 30 4.3–4 252.2	273/273/273	5.00×10^{-4}	2.31×10^{-4}	9.40×10^{-3}	
93Toth_S3[164]	1 381.6–4 006.5	27/27/27	5.00×10^{-3}	1.26×10^{-3}	4.49×10^{-3}	
93Toth_S4[164]	4 077.7–4 106.9	2/2/2	2.00×10^{-2}	1.00×10^{-2}	1.00×10^{-2}	
93Tothb[165]	1 881.1–4 306.7	1 064/1 064/1 064	8.00×10^{-5}	9.65×10^{-5}	1.48×10^{-3}	
93Tothb_S2[165]	1 820.8–4 506.2	1 070/1 070/1 070	2.00×10^{-4}	2.08×10^{-4}	1.06×10^{-2}	
93Tothb_S3[165]	1 898.6–4 458.8	151/151/151	2.00×10^{-3}	1.27×10^{-3}	3.81×10^{-2}	
93Tothb_S4[165]	3 529.7–4 468.7	5/5/5	2.00×10^{-2}	1.00×10^{-2}	1.00×10^{-2}	
70EvWeMaEl[48]	127.48–357.52	2/2/2	1.00×10^{-4}	1.22×10^{-4}	1.43×10^{-4}	
82KaJoHo[166]	501.57–713.79	70/70/67	1.00×10^{-4}	1.47×10^{-4}	4.70×10^{-3}	
85BrTo[113]	1 323.3–1 992.7	71/71/71	1.00×10^{-4}	5.09×10^{-5}	1.73×10^{-3}	0.999 999 936 34
94Tothb[167]	5 754.1–7 671.7	972/971/970	1.00×10^{-4}	1.16×10^{-4}	6.30×10^{-3}	
94Tothb_S2[167]	5 750.9–7 919.9	2 045/2 043/2 034	3.00×10^{-4}	2.55×10^{-4}	2.00×10^{-2}	
94Tothb_S3[167]	5 773.0–7 971.9	522/521/521	3.00×10^{-3}	1.00×10^{-3}	1.50×10^{-2}	
03ZoVa[63]	610.17–4 044.9	889/763/762	1.00×10^{-4}	1.54×10^{-4}	5.84×10^{-3}	
05PtSmSh[66]	5 042.7–5 58 5.3	407/407/407	1.00×10^{-4}	2.93×10^{-5}	9.42×10^{-4}	
15SiHo[20]	7 71 4.8–7 919.9	71/71/71	1.00×10^{-4}	1.13×10^{-4}	1.77×10^{-3}	
18MiMoKaKa[168]	6 667.6–7 449.2	3 550/3 508/3 505	1.00×10^{-4}	2.43×10^{-4}	9.82×10^{-3}	
18ScCiYaGi[33]	6 804.4–7 170.3	572/572/563	1.00×10^{-4}	1.69×10^{-4}	4.97×10^{-3}	
85Johns[169]	18.578–349.76	258/258/258	2.00×10^{-4}	8.60×10^{-5}	4.36×10^{-3}	
86GuRa[170]	5 103.3–5 547.1	234/234/234	2.00×10^{-4}	1.29×10^{-4}	1.96×10^{-2}	0.999 999 933 57
94Toth[171]	11 734–12 638	44/44/44	2.00×10^{-4}	9.28×10^{-4}	2.09×10^{-3}	
94Toth_S2[171]	11 611–12 737	480/480/478	3.00×10^{-4}	7.65×10^{-4}	1.94×10^{-2}	
94Toth_S3[171]	11 638–12 752	250/250/249	3.00×10^{-3}	1.35×10^{-3}	3.33×10^{-2}	
94Toth_S4[171]	11 880–11 934	3/3/3	3.00×10^{-2}	1.00×10^{-2}	1.00×10^{-2}	
05Toth[114]	2 926.5–7 641.9	1 818/1 817/1 817	2.00×10^{-4}	1.00×10^{-4}	6.80×10^{-3}	
08MiAlMeKl[172]	1 901.2–6 598.3	3 769/3 514/3 514	2.00×10^{-4}	4.86×10^{-4}	7.82×10^{-3}	
15HuChTaWa[173]	11 906–12 562	38/38/38	2.00×10^{-4}	2.00×10^{-4}	2.00×10^{-4}	
83ToBr[54]	3 254.1–4 138.8	130/130/130	3.00×10^{-4}	1.70×10^{-4}	6.07×10^{-4}	
99Toth[115]	995.98–4 039.2	794/790/790	3.00×10^{-4}	1.02×10^{-4}	3.12×10^{-3}	
73CaFlGuAm[174]	2 933.7–4 250.9	1 315/1 315/1 315	5.00×10^{-4}	3.57×10^{-4}	2.87×10^{-2}	
98BaGoCaGa[58]	0.741 68–400.22	437/410/408	5.00×10^{-4}	1.21×10^{-3}	1.26×10^{-2}	
07JeDaReTy[175]	4 200.1–6 599.7	5 310/5 310/5 309	5.00×10^{-4}	5.62×10^{-4}	3.44×10^{-2}	
14OsKaPrPe[13]	7 185.4–7 185.6	5/5/5	5.00×10^{-4}	2.69×10^{-4}	6.45×10^{-4}	
17BiWaLoLo[23]	1 850.4–4 340.0	4 129/143/143	5.00×10^{-4}	1.37×10^{-4}	6.57×10^{-3}	
17LoBiWa[24]	1 850.4–3 999.7	4 016/4 015/4 015	5.00×10^{-4}	1.00×10^{-4}	2.16×10^{-2}	
20CaKaYaKy[43]	7 474.6–7 613.9	9/9/9	5.00×10^{-4}	2.65×10^{-3}	8.20×10^{-3}	
81Partridg[176]	16.799–47.055	26/26/26	6.00×10^{-4}	6.35×10^{-4}	4.43×10^{-3}	
07MiLeKaCa[177]	5 912.6–7 014.9	1 374/1 371/1 368	6.00×10^{-4}	8.24×10^{-4}	3.37×10^{-2}	
96BrPl[57]	55.405–4 044.9	592/592/592	7.00×10^{-4}	7.97×10^{-4}	9.87×10^{-3}	
83PiCoCaFl[178]	494.26–4 004.7	2 597/2 592/2 591	8.00×10^{-4}	7.06×10^{-4}	4.60×10^{-2}	
04CoPiVeLa[179]	58.019–475.09	1 708/1 704/1 704	9.00×10^{-4}	3.50×10^{-4}	8.57×10^{-3}	
12MiNaNiVa[80]	6 630.1–8 941.5	516/509/509	9.00×10^{-4}	1.66×10^{-3}	1.66×10^{-2}	
69BePoTo[46]	45.407–84.323	2/2/2	1.00×10^{-3}	1.00×10^{-3}	1.00×10^{-3}	
69BePoTo_S2[46]	83.280–1 340.7	42/42/30	1.00×10^{-2}	1.31×10^{-2}	4.84×10^{-2}	
69BePoTo_S3[46]	207.50–432.30	3/3/0	1.00×10^{-2}	0.00e+00	0.00e+00	

TABLE 1. (*Continued.*)

Segment tag	Range	*A*/*N*/*V*	ESU	MSU	LSU	Recalib. Factor
78KaKaKy[180]	32.955–713.79	416/416/416	1.00×10^{-3}	7.06×10^{-4}	3.16×10^{-2}	
80KaKy[53]	53.445–729.21	427/427/425	1.00×10^{-3}	7.47×10^{-4}	3.80×10^{-2}	
86MaChCaFl[181]	6 443.1–7 830.3	381/381/381	1.00×10^{-3}	2.16×10^{-4}	3.28×10^{-2}	0.999 999 901 82
98EsWaHoRo[182]	720.10–1 397.1	737/737/737	1.00×10^{-3}	7.06×10^{-4}	2.42×10^{-2}	
98Toth[183]	590.60–851.25	49/49/49	1.00×10^{-3}	1.29×10^{-4}	1.07×10^{-3}	
99VaClByLa[184]	1 842.1–2 205.2	63/63/63	1.00×10^{-3}	1.00×10^{-3}	3.40×10^{-3}	0.999 999 741 86
99ZoPoTeLo[185]	933.37–2 500.3	6 810/6 774/6 695	1.00×10^{-3}	7.41×10^{-4}	4.68×10^{-2}	
00ZoPoTeSh[60]	2 497.5–5 987.2	9 613/9 602/9 444	1.00×10^{-3}	2.07×10^{-3}	4.88×10^{-2}	
02MiTyStAl[186]	4 200.1–6 244.7	3 126/3 122/3 122	1.00×10^{-3}	1.05×10^{-3}	2.08×10^{-2}	
02TeBeZoSh[187]	4 878.2–7 552.5	5 589/5 586/5 552	1.00×10^{-3}	2.82×10^{-3}	3.77×10^{-2}	1.000 001 055 60
02TeBeZoSh_S2[187]	5 540.0–6 997.1	682/682/650	5.00×10^{-3}	5.70×10^{-3}	4.61×10^{-2}	
04ShZoPoTe[64]	404.19–1 876.2	787/786/769	1.00×10^{-3}	4.82×10^{-3}	3.99×10^{-2}	
05ToTe[188]	7 423.7–9 595.4	4 221/4 221/4 219	1.00×10^{-3}	6.27×10^{-4}	4.43×10^{-2}	
08ToTe[189]	9 502.0–14 495	10 632/10 097/10 038	1.00×10^{-3}	1.04×10^{-4}	4.94×10^{-2}	
09LiNaKaCa[190]	5 908.7–6 725.7	1 166/1 080/1 080	1.00×10^{-3}	7.00×10^{-4}	1.70×10^{-2}	
11MiKaWaCa[76]	7 408.2–7 919.2	2 045/2 022/2 014	1.00×10^{-3}	6.75×10^{-4}	2.86×10^{-2}	
12LeMiMoKa[79]	6 885.8–7 405.9	2 518/2 460/2 458	1.00×10^{-3}	4.73×10^{-4}	1.58×10^{-2}	
13MiSeSiVa[9]	15 135–15 560	155/150/149	1.00×10^{-3}	2.01×10^{-3}	2.26×10^{-2}	
14CoMaPi[11]	40.517–694.49	6 757/2 464/2 332	1.00×10^{-3}	7.00×10^{-4}	4.00×10^{-2}	
14ReOuMiWa[14]	6 452.9–9 392.5	8 442/8 002/7 994	1.00×10^{-3}	6.77×10^{-4}	3.28×10^{-2}	
15CaMiLoKa[16]	7 911.2–8 336.7	2 056/1 968/1 962	1.00×10^{-3}	1.00×10^{-3}	4.29×10^{-2}	
16MiLeKaMo[22]	5 851.9–6 670.9	2 398/1 841/1 840	1.00×10^{-3}	7.70×10^{-4}	2.21×10^{-2}	
17MoMiKaBe[25]	7 443.6–7 921.2	1 596/1 577/1 575	1.00×10^{-3}	4.12×10^{-4}	2.20×10^{-2}	
19MiKaVaMo[38]	5 694.8–5 990.2	1 051/1 043/1 042	1.00×10^{-3}	5.71×10^{-4}	1.59×10^{-2}	
19MiMoKaKa[39]	5 693.3–5 850.1	514/510/510	1.00×10^{-3}	5.73×10^{-4}	1.38×10^{-2}	
19ReThReMi[40]	6 530.1–7 912.1	1 871/1 840/1 840	1.00×10^{-3}	7.88×10^{-4}	2.00×10^{-2}	
76FlCaMa[50]	2 710.2–6 184.7	3 782/3 780/3 602	1.50×10^{-3}	2.83×10^{-3}	4.73×10^{-2}	
00BrPl[191]	13 818–13 932	6/6/6	1.50×10^{-3}	4.77×10^{-4}	1.08×10^{-2}	
14LiNaKaCa[12]	5 855.7–6 801.6	818/709/709	1.50×10^{-3}	1.50×10^{-3}	1.21×10^{-2}	
97PoZoViTe[192]	373.65–933.62	3 628/3 223/3 096	2.00×10^{-3}	1.00×10^{-3}	4.75×10^{-2}	
98PoZoViTe[193]	13 239–15 995	2 543/736/733	2.00×10^{-3}	2.74×10^{-3}	4.21×10^{-2}	
02ScLeCaBr[61]	13 201–16 499	3 072/3 014/2 930	2.00×10^{-3}	1.09×10^{-3}	4.54×10^{-2}	
03ToTeShZo[62]	9 001.3–12 764	6 378/6 355/6 325	2.00×10^{-3}	8.19×10^{-4}	4.74×10^{-2}	
04MaRoMiNa[194]	6 131.4–26 138	2 375/2 342/2 333	2.00×10^{-3}	1.02×10^{-3}	4.36×10^{-2}	
08LiHo[195]	10 671–10 852	32/32/32	2.00×10^{-3}	2.13×10^{-3}	2.34×10^{-2}	
13LeMiMoKa[7]	5 851.9–6 606.9	3 096/2 916/2 911	2.00×10^{-3}	6.43×10^{-4}	2.59×10^{-2}	
18TaMiWaLi[36]	12 278–12 891	1 590/1 518/1 508	2.00×10^{-3}	1.58×10^{-3}	4.90×10^{-2}	
19LiLiZhWa[37]	12 055–12 260	674/655/651	2.00×10^{-3}	1.87×10^{-3}	4.93×10^{-2}	
20compl	38.532–7 773.4	224/224/224	2.00×10^{-3}	3.23×10^{-4}	1.67×10^{-2}	
20compl_S2	4.330 0–25 197	13 217/13 216/13 188	2.00×10^{-2}	3.70×10^{-3}	4.82×10^{-2}	
02ToTeBrCa[196]	11 788–13 553	1 906/1 906/1 839	2.50×10^{-3}	1.05×10^{-3}	4.81×10^{-2}	
67HaDo[45]	18.570–121.91	73/73/73	3.00×10^{-3}	3.21×10^{-3}	2.92×10^{-2}	
76FlGi[51]	12.683–38.785	11/11/11	3.00×10^{-3}	1.36×10^{-3}	7.15×10^{-3}	
86MaChCaFlb[55]	13 239–15 964	1 980/1 979/1 890	3.00×10^{-3}	3.00×10^{-3}	4.08×10^{-2}	
02BrToDu[197]	9 676.9–11 383	2 594/2 594/2 592	3.00×10^{-3}	5.91×10^{-4}	4.20×10^{-2}	
05CoBeCaCo[198]	373.65–1 999.8	16 546/13 223/12 943	3.00×10^{-3}	3.81×10^{-3}	4.99×10^{-2}	
05ToNaZoSh[199]	9 250.2–25 232	15 621/15 511/15 393	3.00×10^{-3}	2.20×10^{-3}	4.94×10^{-2}	
06ZoOvShPo[67]	404.19–4 272.8	1 461/1 460/1 457	3.00×10^{-3}	6.66×10^{-3}	3.99×10^{-2}	
07MaToCa[68]	11 523–12 806	1 553/1 507/1 448	3.00×10^{-3}	2.45×10^{-3}	4.38×10^{-2}	
12DoTeOrCh[78]	6 530.1–6 949.7	304/304/304	3.00×10^{-3}	9.61×10^{-4}	1.61×10^{-2}	1.000 002 800 28
15MiSeSi[19]	15 135–16 005	495/338/332	3.00×10^{-3}	3.52×10^{-3}	3.63×10^{-2}	
18SeSiVaLa[35]	16 609–17 061	216/214/212	3.00×10^{-3}	3.00×10^{-4}	1.00×10^{-2}	
19SeSiLaDu[41]	19 560–19 920	91/80/80	3.00×10^{-3}	3.12×10^{-4}	2.55×10^{-3}	

TABLE 1. (*Continued.*)

Segment tag	Range	*A*/*N*/*V*	ESU	MSU	LSU	Recalib. Factor
89ChMaFlCa[200]	9 603.7–11 481	2 393/2 393/2 393	4.00×10^{-3}	7.71×10^{-4}	4.34×10^{-2}	
99CaJeVaBe[201]	13 185–21 390	5 698/5 693/5 540	4.00×10^{-3}	1.27×10^{-3}	4.65×10^{-2}	
00ByNaVo[59]	18 026–19 106	112/112/108	4.00×10^{-3}	3.58×10^{-3}	3.22×10^{-2}	
00ZoBePoTe[202]	21 411–25 225	297/297/252	4.00×10^{-3}	2.61×10^{-3}	4.07×10^{-2}	
05DuGhZoTo[203]	25 196–25 337	47/47/47	4.00×10^{-3}	4.00×10^{-3}	2.50×10^{-2}	
06MaNaKaBy[204]	11 335–12 843	1 280/1 277/1 268	4.00×10^{-3}	2.30×10^{-3}	4.96×10^{-2}	
08CaMiLi[205]	12 747–13 558	1 121/1 096/1 076	4.00×10^{-3}	3.65×10^{-3}	4.98×10^{-2}	
14SiSeVaBy[15]	15 529–16 062	440/438/433	4.00×10^{-3}	2.92×10^{-3}	3.22×10^{-2}	
69FrRa[47]	3 355.7–4 025.4	476/476/438	5.00×10^{-3}	6.03×10^{-3}	4.75×10^{-2}	
73PuRa[206]	3 261.0–4 193.9	33/33/30	5.00×10^{-3}	9.93×10^{-3}	4.64×10^{-2}	
77FlCaMaGu[207]	4 200.2–5 554.9	448/445/445	5.00×10^{-3}	2.06×10^{-3}	3.54×10^{-2}	
79FlCaNaCh[208]	8 060.1–9 366.6	1 219/1 219/1 195	5.00×10^{-3}	3.65×10^{-3}	4.66×10^{-2}	
80CaFlMa[209]	5 937.4–6 443.1	79/79/79	5.00×10^{-3}	2.16×10^{-3}	4.26×10^{-2}	
85CaFlMaCh[210]	16 548–25 173	989/989/986	5.00×10^{-3}	2.16×10^{-3}	4.47×10^{-2}	
88MaChFlCa[211]	8 057.9–9 481.8	1 667/1 667/1 667	5.00×10^{-3}	7.65×10^{-4}	4.46×10^{-2}	
92DaMaCaFl[212]	1 092.5–1 844.0	159/159/159	5.00×10^{-3}	2.58×10^{-3}	2.44×10^{-2}	
92DaMaCaFlb[213]	855.91–1 848.8	216/216/216	5.00×10^{-3}	2.48×10^{-3}	2.97×10^{-2}	
92MaDaCaFl[214]	811.56–1 265.1	80/80/80	5.00×10^{-3}	5.17×10^{-3}	2.44×10^{-2}	
96PoBuGuZh[215]	407.31–921.40	585/585/585	5.00×10^{-3}	5.00×10^{-4}	2.51×10^{-2}	
97PoTeBe[216]	385.08–874.26	353/353/353	5.00×10^{-3}	5.00×10^{-4}	2.83×10^{-2}	
01ByNaSiVo[217]	1 027.5–13 936	106/104/104	5.00×10^{-3}	1.18×10^{-3}	1.42×10^{-2}	
03NaCa[218]	9 518.9–10 009	641/637/635	5.00×10^{-3}	2.53×10^{-3}	4.32×10^{-2}	
05KaMaNaCa[219]	13 312–13 378	273/273/258	5.00×10^{-3}	2.96×10^{-3}	3.41×10^{-2}	
06PePoSeSi[220]	9 388.0–9 451.2	96/95/91	5.00×10^{-3}	7.01×10^{-3}	4.79×10^{-2}	
06PePoSeSi_S2[220]	9 392.5–9 450.6	47/46/34	1.00×10^{-2}	2.01×10^{-2}	4.96×10^{-2}	
06ZoShPoBa[221]	2 000.2–4 749.9	15 045/14 020/13 745	5.00×10^{-3}	7.15×10^{-3}	4.91×10^{-2}	
12Boyarkin[222]	11 174–11 333	3/3/3	5.00×10^{-3}	1.00×10^{-2}	2.98×10^{-2}	
12VaMiSeSi[83]	13 459–14 440	446/439/438	5.00×10^{-3}	3.67×10^{-3}	4.41×10^{-2}	
18MiSeSi[30]	16 470–17 180	721/702/695	5.00×10^{-3}	3.19×10^{-3}	4.57×10^{-2}	
18SiSePoBy[34]	19 488–20 495	461/459/455	5.00×10^{-3}	4.38×10^{-3}	3.95×10^{-2}	
18CzFuCsEc[27]	6 600.5–7 048.5	4 080/4 080/4 076	6.00×10^{-3}	2.20×10^{-3}	4.43×10^{-2}	
75ToMa[223]	6 952.3–7 508.4	852/852/852	7.00×10^{-3}	6.63×10^{-3}	4.39×10^{-2}	
79WiScGeGi[52]	13 584–13 987	62/62/59	7.00×10^{-3}	3.42×10^{-3}	2.14×10^{-2}	1.000 000 631 49
97PoZoTeLo[224]	928.68–2 323.7	1 514/1 514/1 513	8.00×10^{-3}	8.00×10^{-4}	3.43×10^{-2}	
11BeMiCa[225]	13 543–14 073	174/174/170	8.00×10^{-3}	7.70×10^{-3}	3.53×10^{-2}	
18RuFoScJo[32]	6 250.1–6 666.5	2 854/2 854/2 810	1.00×10^{-2}	1.02×10^{-2}	4.88×10^{-2}	
97FlCaByNa[226]	11 523–12 837	1 656/1 619/1 607	2.00×10^{-2}	2.00×10^{-3}	2.84×10^{-2}	
08ZoShOvPo[116]	4 251.4–12 361	28 885/28 761/27 808	2.00×10^{-2}	1.07×10^{-2}	4.98×10^{-2}	
20extra[3]	554.16–21 411	138/138/127	2.00×10^{-2}	1.00×10^{-2}	3.51×10^{-2}	
08GrMaZoSh[119]	13 531–17 448	413/405/386	3.00×10^{-2}	2.69×10^{-2}	4.83×10^{-2}	
09GrBoRiMa[120]	10 305–14 619	470/467/429	3.00×10^{-2}	3.00×10^{-2}	4.13×10^{-2}	

[a]Tags denote segments used in this study. Bold entries are new segments compared to Part III. The column "Range" indicates the range (in cm^{-1}) corresponding to validated wavenumbers within the transition list. *A* is the number of assigned transitions, *N* is the number of non-redundant lines (with distinct wavenumbers or labels), and *V* is the number of validated transitions obtained at the end of the xMARVEL analysis. In the heading of this table, ESU, MSU, and LSU denote the estimated, the median, and the largest segment uncertainties in cm^{-1}, respectively. The value "0.00e+00" in the sixth column indicates that the associated LSU is undefined. Rows are arranged in the order of the ESUs with the restriction that the segments of the same data source should be listed consecutively.

After completion of the resistance analysis,[87,107] 13 676, 3657, 52, and 1819 rovibrational states of the PCs are specified as R^+, R^-, S, and U, respectively. The maximum *J* value is 42 for the whole set of energy levels within the PCs. The energy of the highest-lying rovibrational state within the W2020 database is 41 143.8 cm^{-1}. The W2020 empirical energy levels are presented in the supplementary material.

Since the publication of the Part III database in 2013, several tens of thousands of new lines were detected, remeasured, or reassigned. It is notable that they determine only about 800 new energy levels. Thus, only a small fraction of the measured transitions leads to new rovibrational states, even though the energies of the great majority of the bound rovibrational states

of $H_2{}^{16}O$ are still not known empirically ($H_2{}^{16}O$ has close to one million bound rovibrational states,[31] of which fewer than 20 000 are determined by experiments). In this sense, the most useful new sources are 18RuFoScJo,[32] 14CoMaPi,[11] and 15CaMiLoKa,[16] with 86, 79, and 63 new rovibrational states, respectively.

Table 2 shows the (empirical) vibrational band origins (VBOs) derived from the W2020 transition database. The uncertainties of the VBOs of W2020 are significantly better than those determined in Part III. The vibrational fundamentals of $H_2{}^{16}O$ are now known with remarkable accuracy ($\approx 10^{-5}$ cm^{-1}). In fact, all the VBOs with $P = 1$, 2, and 3, where $P = 2v_1 + v_2 + 2v_3$ is the polyad number, have a similarly high precision. The complete list of the 240 vibrational bands along with the polyad numbers and the number of xMARVEL energy levels associated with the specific bands is given in the supplementary material.

TABLE 2. Vibrational band origins (VBOs) of $H_2{}^{16}O$ present in the W2020 dataset[a]

$(v_1\ v_2\ v_3)$	VBO (cm^{-1})	$(v_1\ v_2\ v_3)$	VBO (cm^{-1})	$(v_1\ v_2\ v_3)$	VBO (cm^{-1})
(0 0 0)	0.0	(3 0 1)	13 830.936 71(35)	(10 0 0)	29 810.850(30)
(0 1 0)	1 594.746 168(28)	(1 2 2)	13 910.895(12)	(8 0 2)	31 071.570(30)
(0 2 0)	3 151.629 947(19)	(0 2 3)	14 066.193 67(20)	(10 1 0)	31 207.090(30)
(1 0 0)	3 657.053 161 6(76)	(2 0 2)	14 221.158 9(10)	(11 0 0)	31 909.679(30)
(0 0 1)	3 755.928 574 3(69)	(1 0 3)	14 318.812 66(63)	(11 1 0)	33 144.709(30)
(0 3 0)	4 666.789 706(72)	(0 0 4)	14 537.504 2(11)	(11 0 1)	33 835.222(30)
(1 1 0)	5 234.975 47(49)	(0 7 1)	13 835.372 4(10)	(12 0 0)	33 835.249(30)
(0 1 1)	5 331.267 211(10)	(1 5 1)	14 647.977 3(18)	(9 0 3)	35 509.677(30)
(0 4 0)	6 134.015 33(42)	(3 3 0)	15 108.238 6(20)	(9 1 3)	36 739.777(30)
(1 2 0)	6 775.093 03(15)	(2 3 1)	15 119.028 5(13)	(10 1 2)	36 740.597(30)
(0 2 1)	6 871.520 14(26)	(4 1 0)	15 344.503 2(19)	(13 0 0)	35 585.957(30)
(2 0 0)	7 201.540 31(10)	(3 1 1)	15 347.957 06(10)	(12 0 1)	35 586.007(30)
(1 0 1)	7 249.818 36(13)	(0 3 3)	15 534.709 4(10)	(12 2 0)	36 179.317(30)
(0 0 2)	7 445.045 33(12)	(2 1 2)	15 742.803(11)	(13 1 0)	36 684.047(30)
(0 5 0)	7 542.382(21)	(1 1 3)	15 832.765 66(30)	(12 1 1)	36 684.877(30)
(1 3 0)	8 273.975 85(47)	(2 4 1)	16 546.318 6(30)	(11 3 1)	37 309.847(30)
(0 3 1)	8 373.851 39(11)	(3 2 1)	16 821.631(10)	(12 3 0)	37 311.277(30)
(2 1 0)	8 761.582 19(11)	(4 2 0)	16 823.318 5(30)	(14 0 0)	37 122.697(30)
(1 1 1)	8 806.998 91(11)	(4 0 1)	16 898.842 19(30)	(13 0 1)	37 122.717(30)
(0 1 2)	9 000.136 6(13)	(2 2 2)	17 227.379 5(30)	(13 2 0)	37 765.647(30)
(0 6 0)	8 869.951(20)	(1 2 3)	17 312.551 3(30)	(14 1 0)	38 153.247(30)
(1 4 0)	9 724.187 3(20)	(3 0 2)	17 458.214 1(30)	(13 1 1)	38 153.307(30)
(0 4 1)	9 833.584 06(10)	(2 0 3)	17 495.528 0(30)	(12 1 2)	40 044.567(42)
(2 2 0)	10 284.364 9(10)	(1 0 4)	17 748.106 7(30)	(11 1 3)	40 044.706(32)
(1 2 1)	10 328.730 20(17)	(3 3 1)	18 265.820 6(15)	(15 0 0)	38 462.517(30)
(0 2 2)	10 521.759 7(10)	(5 1 0)	18 392.777 5(30)	(14 0 1)	38 462.537(30)
(3 0 0)	10 599.687 27(21)	(4 1 1)	18 393.314 1(15)	(14 2 0)	39 123.767(30)
(2 0 1)	10 613.363 3(16)	(1 3 3)	18 758.633 4(10)	(12 0 3)	40 704.191(32)
(1 0 2)	10 868.875 93(21)	(2 1 3)	18 989.959 9(30)	(14 1 1)	39 390.217(30)
(0 0 3)	11 032.405 16(10)	(3 4 1)	19 679.201(17)	(15 1 0)	39 390.257(30)
(0 5 1)	11 242.777 2(10)	(5 0 1)	19 781.103 0(11)	(13 3 1)	40 262.036(32)
(2 3 0)	11 767.388 3(10)	(6 0 0)	19 781.322 6(30)	(15 0 1)	39 574.537(30)
(1 3 1)	11 813.207 17(15)	(4 2 1)	19 865.288 2(74)	(16 0 0)	39 574.547(30)
(0 3 2)	12 007.776 2(14)	(2 2 3)	20 442.777 4(30)	(14 2 1)	40 226.301(19)
(3 1 0)	12 139.315 73(10)	(3 0 3)	20 543.128 6(30)	(16 1 0)	40 370.547(42)
(2 1 1)	12 151.254 86(10)	(5 1 1)	21 221.827 3(30)	(15 1 1)	40 370.816(32)
(1 1 2)	12 407.662 22(19)	(4 3 1)	21 314.448 2(30)	(17 0 0)	40 437.227(42)
(0 1 3)	12 565.006 85(11)	(7 0 0)	22 529.291 9(84)	(16 0 1)	40 437.246(32)
(0 6 1)	12 586.229 9(20)	(6 0 1)	22 529.440 6(17)	(15 2 1)	41 121.641(32)
(2 4 0)	13 204.787 2(27)	(7 0 1)	25 120.277 8(17)	(17 1 0)	40 984.637(42)
(1 4 1)	13 256.158(15)	(5 3 2)	27 502.660(30)	(17 0 1)	40 945.728(32)
(3 2 0)	13 640.716(20)	(6 1 2)	27 574.910(30)	(18 0 0)	40 947.487(42)
(2 2 1)	13 652.653 90(50)	(9 0 0)	27 540.690(10)	(18 0 1)	41 100.088(32)
(4 0 0)	13 828.277 3(17)	(9 1 0)	28 934.140(30)	(19 0 0)	41 101.337(42)

[a]$(v_1\ v_2\ v_3)$ denotes a specific vibrational band, where v_1, v_2, and v_3 are the standard normal-mode quantum numbers describing the corresponding vibrational state. The uncertainties related to the last digits of the VBOs are provided in parentheses.

4.2. Validation of the W2020 database

As an independent validation of the transition wavenumbers, the derived xMARVEL energies, and the labels collated into the W2020 database, systematic and mostly automated comparisons were made with the results of variational nuclear-motion computations[31,109] and previously reported energies, mostly corresponding to effective Hamiltonian (EH) fits.[11,179,227,228] These comparisons were executed in order to exclude those transitions from the W2020 database that would lead to energy levels with large deviations from well-established first-principles or EH values.

4.2.1. Comparison with first-principles energy levels

As described for task (c) of Sec. 3, the xMARVEL energy levels were matched with their first-principles counterparts listed in both the recent PoKaZaTeL[31] and the older BT2[109] energy lists. An important property of the W2020 rovibrational energy-level set is that it is complete up to 9724 cm^{-1}. This increases the completeness limit from the Part III value of about 7500 cm^{-1}.[93]

The unsigned (energy) deviations (UD) for these datasets are plotted in Fig. 2. Although the median values of the UDs are 0.085 cm^{-1} and 0.110 cm^{-1} for PoKaZaTeL and BT2, respectively, the xMARVEL–PoKaZaTeL energy differences become significantly smaller than their xMARVEL–BT2 counterparts above 15 000 cm^{-1}. Partitioning the 0–30 000 cm^{-1} range, where energy levels are present from both the PoKaZaTeL and the BT2 energy lists, into six intervals of equal widths of 5000 cm^{-1}, the following median unsigned deviations are obtained for BT2/PoKaZaTeL: 0.07/0.03 cm^{-1}, 0.09/0.06 cm^{-1}, 0.11/0.11 cm^{-1}, 0.13/0.09 cm^{-1}, 0.23/0.05 cm^{-1}, and 0.50/0.08 cm^{-1}.

These comparisons verify that each W2020 state has a variational counterpart with a deviation not larger than 1.5 cm^{-1} up to 30 000 cm^{-1}. For the PoKaZaTeL dataset, the highest UD is 1.32 cm^{-1}, but almost all UDs are well below 1 cm^{-1} in the 0–30 000 cm^{-1} range (see Fig. 2). The larger xMARVEL–PoKaZaTeL deviations (~10 cm^{-1}) above 30 000 cm^{-1} indicate that further empirical adjustment of the spectroscopic PES of $H_2{}^{16}O$ is required to secure that *all* first-principles PoKaZaTeL energies are below the venerable 0.03 cm^{-1} limit, characteristic of the 0–5000 cm^{-1} range. It is remarkable how well the PoKaZaTeL energies reproduce nearly all of their W2020 counterparts with deviations less than the level spacings, allowing unambiguous matching for all the xMARVEL states.

4.2.2. Comparison with 01LaCoCa–04CoPiVeLa

Following the first-principles validation, the empirical Part III and W2020 energy values were compared with those obtained in 01LaCoCa[227] and 04CoPiVeLa.[179] To find the appropriate pairs, we relied exclusively on the J values and the parities of the rovibrational states (that is, the normal-mode vibrational and rigid-rotor rotational labels were not utilized directly in the matching procedure).

The UDs for the (Part III, 01LaCoCa–04CoPiVeLa) and (W2020, 01LaCoCa–04CoPiVeLa) pairs are shown in Fig. 3 as a function of energy. The median and the largest UDs are $6.72 \times 10^{-4}/1.16 \times 10^{-3}$ and $9.78 \times 10^{-2}/1.85 \times 10^{-1}$ cm^{-1} for the W2020/Part III energy levels, respectively, implying that the W2020 dataset represents a significant improvement over the Part III database. These results also implicitly confirm the considerable accuracy of the energy levels of 01LaCoCa[227] and 04CoPiVeLa.[179]

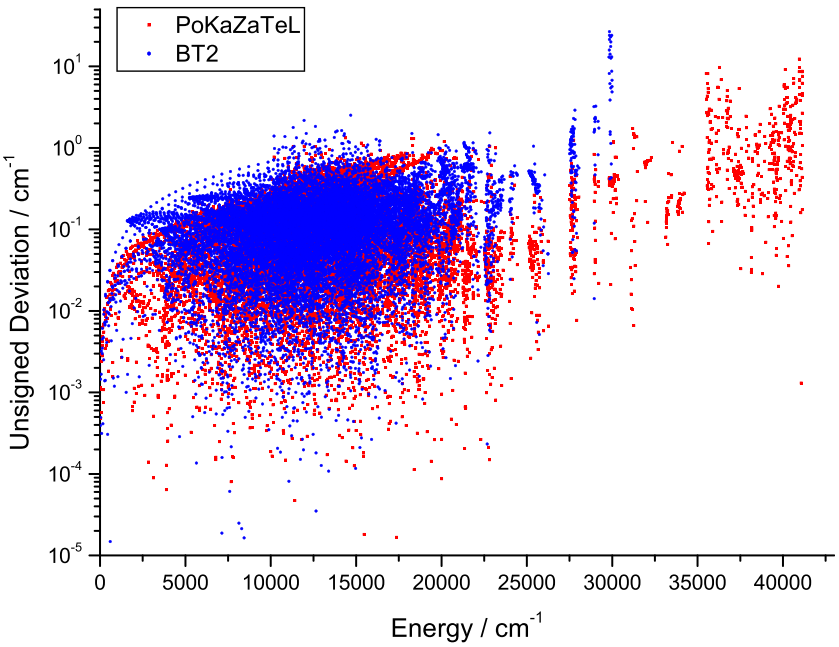

FIG. 2. Unsigned deviations of the BT2 (blue dots, Ref. 109) and PoKaZaTeL (red squares, Ref. 31) states from their W2020 counterparts.

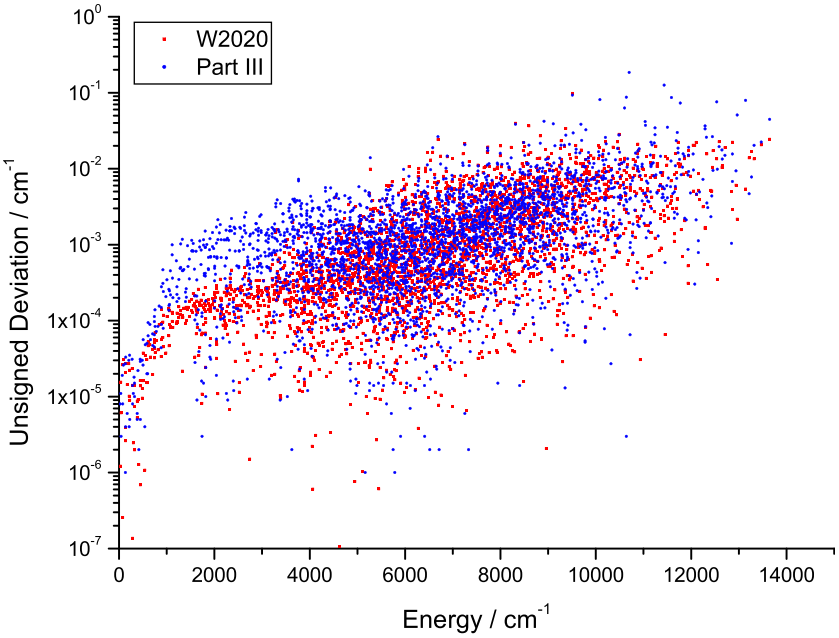

FIG. 3. Unsigned deviations of the W2020 and Part III[3] energy levels, denoted with red squares and blue dots, respectively, from their 01LaCoCa[227]–04CoPiVeLa[179] counterparts.

4.2.3. Comparison with Part III energy levels

Since the 01LaCoCa–04CoPiVeLa dataset does not cover the whole energy range represented by the W2020 database, it is important to evaluate the differences between the W2020 energy values and their Part III[3] analogs. The list of those 213 Part III levels that could not be matched within 0.1 cm^{-1} can be found in the supplementary material. Some of the 213 states are not present in the W2020 database because they caused large deviations from the PoKaZaTeL energies and therefore were excluded from W2020. In most other cases, another subset of transitions, in conflict with those chosen in Part III, were selected based on the differences, down to a few times 0.01 cm^{-1}, from the PoKaZaTeL energies.

The pattern of the UDs, calculated for the matched (Part III, W2020) twins, is shown in Fig. 4. The overwhelming majority of the UDs (14 370) are smaller than 0.005 cm^{-1}, demonstrating that the Part III and the W2020 data agree adequately. Nonetheless, the number of levels with 0.005 cm^{-1} < UD ≤ 0.05 cm^{-1} and 0.05 cm^{-1} < UD ≤ 0.1 cm^{-1} (3778 and 124, respectively) indicates that the improvement over the Part III data is significant.

4.2.4. Comparison with 14CoMaPi

Figure 5 displays the unsigned deviations of the 14CoMaPi[11] energies from their W2020 counterparts. While the overall agreement is remarkably good, there are a few energy levels between 9000 and 13 000 cm^{-1} where the UDs are larger than 1.0 cm^{-1}. Since the variationally computed energies, from both the PoKaZaTeL and the BT2 lists, confirm the W2020 energies to a few 0.01 cm^{-1}, there is no reason to exclude the corresponding transitions from the xMARVEL analysis. In other words, the effective-Hamiltonian-based predictions appear to be slightly incorrect for these outliers, typically having K_a > 27. It is likely that these deviant effective-Hamiltonian-based estimates are due to the lack of transitions characterized with high J and K_a values used during the refinement of the spectroscopic parameters in the bending rotational Hamiltonian of 14CoMaPi.

4.2.5. Comparison with JPL data

On the JPL (Jet Propulsion Laboratory) website[228] a list of energy values is maintained, complemented with a timestamp of "Oct 31 21:54:56 2005," which were deduced from a fit with an Euler-type Hamiltonian. The parameterization of this model is quite similar to that introduced in 05PiPeMi.[229]

Figure 6 exhibits the unsigned deviations of the JPL data[228] from their W2020 analogs up to J = 22. Although there are extrapolated energy values for J = 23 in the JPL set, we decided to ignore them during this analysis due to their considerably increased deviations. As can be seen from Fig. 6, most of the JPL energies reproduce well, better than 0.01 cm^{-1}, their xMARVEL counterparts. Similar to 14CoMaPi,[11] the W2020 energies corresponding to the outlier points of this figure were carefully checked and found to be dependable within the stated uncertainties, suggesting that there are issues for these energy values within the JPL list.

4.3. HITRAN 2016 issues

Employing the W2020 database of $H_2{}^{16}O$ transitions, one can check the reliability of the data of the canonical spectroscopic database HITRAN 2016.[88] The latest HITRAN version[88] of the $H_2{}^{16}O$ line list contains 141 360 transitions in the range of 0.072–25 710.82 cm^{-1}. Thus, HITRAN 2016[88] is more limited than W2020 both in its wavenumber range and in the number of validated transitions. While

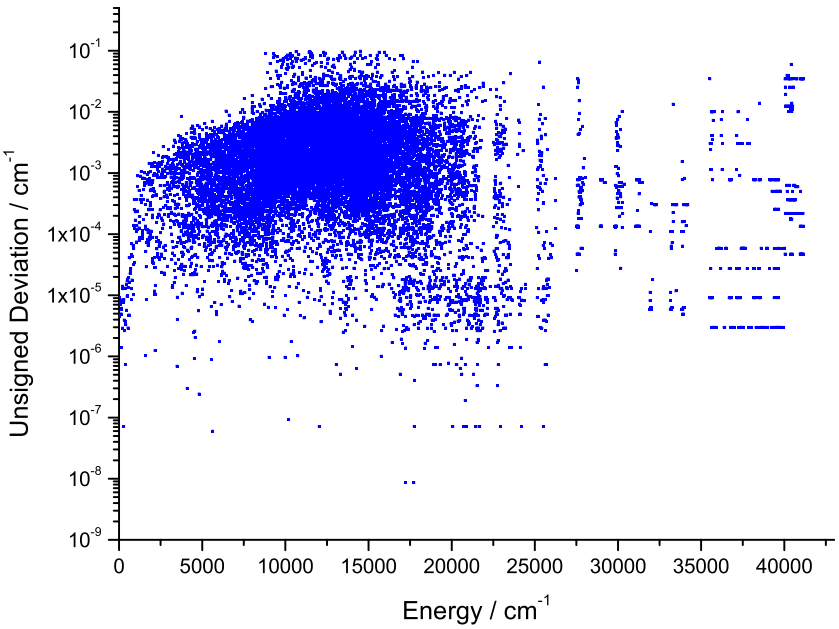

FIG. 4. Unsigned deviations of the Part III[3] energy levels from their W2020 counterparts. The states (both Part III and W2020) that could not be matched within 0.1 cm^{-1} are listed in the supplementary material.

some of the W2020 data are not relevant for atmospheric modeling, most of them certainly are.

Since xMARVEL works with positions and quantum labels of the measured transitions and it results in empirical energy levels, we examine three types of information found in the HITRAN 2016 database. After the comparison of W2020 with HITRAN 2016, we could divide the issues found into the following four categories:

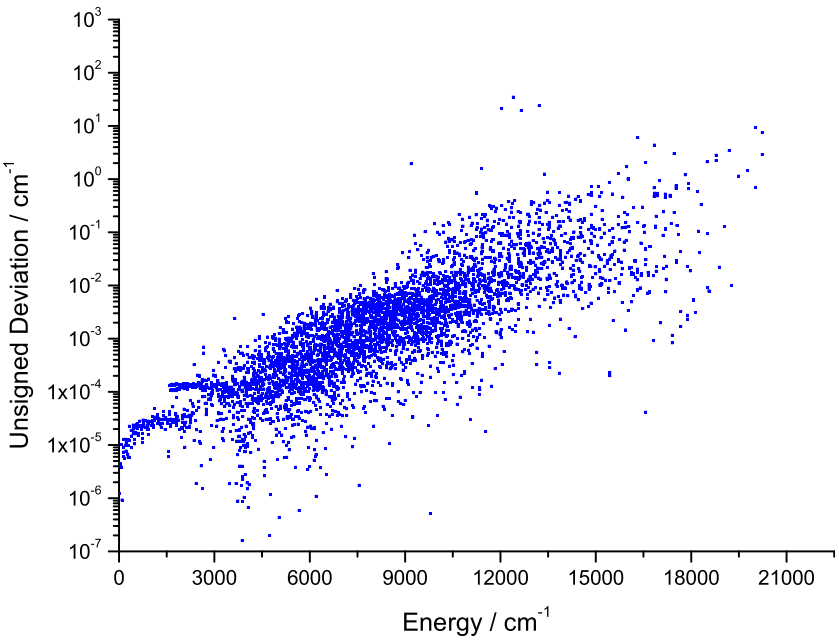

FIG. 5. Unsigned deviations of the 14CoMaPi[11] energy levels from their W2020 counterparts.

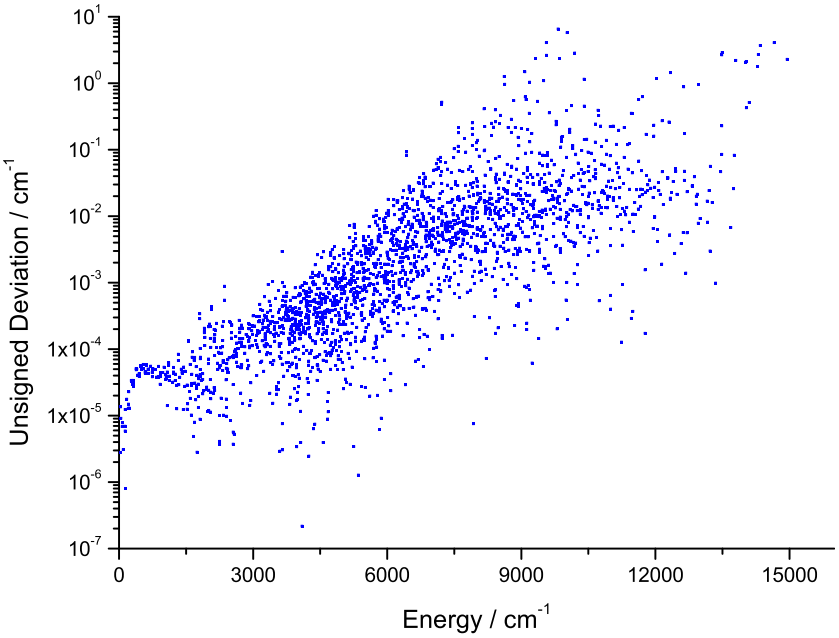

FIG. 6. Unsigned deviations of the JPL[228] energy levels from their W2020 counterparts.

I. **Inconsistency in the lower-state energies**. Energy values of the lower states are given explicitly in HITRAN 2016. Although we are aware of the fact that, for HITRAN 2016, the transitions and the lower-state energies were collected from a number of different sources, the issue that the energy values of the same quantum state might differ by more than 0.1 cm^{-1} should be remedied. Therefore, we suggest that a single energy value should be used for the lower states, preferably taken from the W2020 dataset, in the next edition of the HITRAN database.

II. **Forbidden transitions**. Employing the rovibrational symmetry of the lower and upper states, 31 forbidden transitions were found in the HITRAN 2016 database of which 27 could be corrected. The forbidden lines found and our recommendations how to cure the problems observed are listed in the supplementary material.

III. **Missing upper labels**. The HITRAN 2016 database contains 5639 $H_2{}^{16}O$ transitions without labels for the upper states. The database indicates the missing labels with the descriptor −2. For 1463 cases, we found feasible W2020 recommendations. This relatively small number shows that, in most cases, these lines are likely taken from theoretical calculations, and thus, we need new measurements to properly characterize these transitions. The list of the HITRAN 2016 lines with missing labels and the corresponding W2020 recommendations can be found in the supplementary material.

IV. **Inaccurate line positions and labeling conflicts**. The safest matching of the HITRAN 2016 and W2020 lines is achieved if it is governed by the quantum numbers of the lower and upper states given in HITRAN 2016 for the transition. We accept a match between a HITRAN 2016 line and its W2020 counterpart if their deviation is less than $\max(10^{-6}\times E^{\mathrm{up}}_{\mathrm{HITRAN}}, \delta_{\mathrm{W2020}})$, where $E^{\mathrm{up}}_{\mathrm{HITRAN}}$ is the energy value of the upper state in HITRAN 2016 and δ_{W2020} is the uncertainty of the W2020 prediction. There are two possible reasons why the HITRAN 2016 and W2020 line positions do not match. It is possible that the positions appear to be different because W2020 uses a label different from the HITRAN 2016 one. In this case, the HITRAN 2016 lines should be reassigned and given the W2020 label of the upper state, assuming that the labels of the lower states agree. It is also possible that a HITRAN 2016 line comes from a theoretical source or that its W2020 counterpart is considerably more accurate. In this case, the next edition of HITRAN should use the W2020 line position. We found altogether 5539 problematic lines in HITRAN 2016. In 878 cases, the labels should be reassigned, while for the rest of the problematic cases, the line positions should be changed to the W2020 positions. It is important to emphasize that the largest intensity in these problematic cases is 5×10^{-24} cm $molecule^{-1}$, which means that all strong lines in HITRAN 2016 are correct, though the W2020 line positions may have considerably higher accuracy.

4.4. Highly accurate pure rotational lines

A common feature of most present-day line-by-line spectroscopic databases, including HITRAN 2016,[88] is that they are based almost exclusively on lines obtained from Doppler-broadened spectra. The usual Doppler linewidth is about 1–5 GHz, strongly limiting the accuracy of the line centers of the high-resolution spectra measured. Modern laser spectroscopy measurements, relying on frequency combs, cavity enhancement, saturation, and other recent experimental advances, allow Doppler-free measurement of certain lines. The accuracy of these measurements approaches the 1 kHz region, though, in principle, it can be even better.

As shown in Table 3, containing $H_2{}^{16}O$ rotational lines protected by certain bodies of the National Academies of Sciences, Engineering,

TABLE 3. Pure rotational lines of $H_2{}^{16}O$ under protection by the National Academies of Sciences, Engineering, and Medicine and their various experimental and empirical determinations as given in the W2020 dataset.[a]

f(NASEM) (GHz)	$(v_1' v_2' v_3')J'_{K_a',K_c'} \leftarrow (v_1'' v_2'' v_3'')J''_{K_a''K_c''}$	*f*(xMARVEL) (GHz)	*f*(expt.) (GHz)
22.235	$(0\,0\,0)6_{1,6} \leftarrow (0\,0\,0)5_{2,3}$	22.235 079 85(5)	22.235 079 85(5)[126]
183.310	$(0\,0\,0)3_{1,3} \leftarrow (0\,0\,0)2_{2,0}$	183.310 087(1)	183.310 087(1)[129]
			183.310 091(3)[128]
			183.310 08(1)[65]
			183.310 07(1)[132]
			183.310 15(6)[133]
			183.310 1(1)[148]
325.153	$(0\,0\,0)5_{1,5} \leftarrow (0\,0\,0)4_{2,2}$	325.152 901(3)	325.152 902(1)[144]
			325.152 899(1)[129]
			325.152 90(1)[144]
			325.152 89(1)[130]
			325.152 9(1)[148]
380.197	$(0\,0\,0)4_{1,4} \leftarrow (0\,0\,0)3_{2,1}$	380.197 359 8(1)	380.197 359 8(1)[127]
			380.197 356(5)[129]
			380.197 365(5)[130]
			380.197 353(7)[131]
439.151	$(0\,0\,0)6_{4,3} \leftarrow (0\,0\,0)5_{5,0}$	439.150 794 8(3)	439.150 794 8(3)[127]
			439.150 795(5)[129]
			439.150 81(1)[131]
448.001	$(0\,0\,0)4_{2,3} \leftarrow (0\,0\,0)3_{3,0}$	448.001 077 5(5)	448.001 077 5(5)[127]
			448.001 09(1)[131]
474.689	$(0\,0\,0)5_{3,3} \leftarrow (0\,0\,0)4_{4,0}$	474.689 108(1)	474.689 108(1)[129]
			474.689 09(1)[131]
556.936	$(0\,0\,0)1_{1,0} \leftarrow (0\,0\,0)1_{0,1}$	556.935 987 7(3)	556.935 987 7(3)[127]
			556.935 985(2)[56]
			556.936 00(1)[129]
620.700	$(0\,0\,0)5_{3,2} \leftarrow (0\,0\,0)4_{4,1}$	620.700 954 9(6)	620.700 954 9(6)[127]
			620.700 97(2)[144]
752.033	$(0\,0\,0)2_{1,1} \leftarrow (0\,0\,0)2_{0,2}$	**752.033 12(1)**	752.033 11(1)[72]
			752.033 10(7)[143]
			752.033 1(1)[144]
			752.033 2(1)[148]
			752.033 3(2)[153]
916.172	$(0\,0\,0)4_{2,2} \leftarrow (0\,0\,0)3_{3,1}$	**916.171 447(9)**	916.171 41(7)[143]
			916.171 6(1)[135]
			916.171 6(1)[136]
970.315	$(0\,0\,0)5_{2,4} \leftarrow (0\,0\,0)4_{3,1}$	**970.315 045(9)**	970.315 02(2)[135]
			970.315 02(2)[136]
			970.315 05(3)[144]
			970.314 97(7)[143]
987.927	$(0\,0\,0)2_{0,2} \leftarrow (0\,0\,0)1_{1,1}$	**987.926 792(8)**	987.926 76(2)[136]
			987.926 76(3)[135]
			987.926 76(3)[144]
			987.926 74(7)[143]
			987.927 4(5)[169]
1097.365	$(0\,0\,0)3_{1,2} \leftarrow (0\,0\,0)3_{0,3}$	**1097.364 862(6)**	1097.364 79(7)[143]
			1097.364 79(8)[145]
			1097.364 9(1)[144]
1113.343	$(0\,0\,0)1_{1,1} \leftarrow (0\,0\,0)0_{0,0}$	**1113.343 014(7)**	1113.343 01(5)[144]
			1113.342 96(7)[143]
1153.127	$(0\,0\,0)3_{1,2} \leftarrow (0\,0\,0)2_{2,1}$	**1153.126 820(6)**	1153.126 82(7)[143]
			1153.126 82(8)[145]

TABLE 3. (*Continued.*)

f(NASEM) (GHz)	$(v_1' v_2' v_3')J'_{K_a',K_c'} \leftarrow (v_1'' v_2'' v_3'')J''_{K_a''K_c''}$	*f*(xMARVEL) (GHz)	*f*(expt.) (GHz)
1158.324	$(0\,0\,0)6_{3,4} \leftarrow (0\,0\,0)5_{4,1}$	**1158.323 84(1)**	1158.323 85(3)[144] 1158.323 84(5)[144] 1158.323 7(1)[143]
1162.912	$(0\,0\,0)3_{2,1} \leftarrow (0\,0\,0)3_{1,2}$	**1162.911 606(8)**	1162.911 61(2)[144] 1162.911 59(7)[143] 1162.911 60(8)[145]
1207.639	$(0\,0\,0)4_{2,2} \leftarrow (0\,0\,0)4_{1,3}$	**1207.638 693(9)**	1207.638 71(7)[143] 1207.638 73(7)[144]
1228.789	$(0\,0\,0)2_{2,0} \leftarrow (0\,0\,0)2_{1,1}$	**1228.788 725(7)**	1228.788 77(7)[143] 1228.788 72(7)[144]
1322.065	$(0\,0\,0)6_{2,5} \leftarrow (0\,0\,0)5_{3,2}$	**1322.064 74(1)**	1322.064 74(5)[10] 1322.064 80(7)[143]
1410.618	$(0\,0\,0)5_{2,3} \leftarrow (0\,0\,0)5_{1,4}$	**1410.618 033(9)**	1410.618 07(7)[143] 1410.618 07(8)[145] 1410.618 2(5)[169]
1440.782	$(0\,0\,0)7_{2,6} \leftarrow (0\,0\,0)6_{3,3}$	**1440.781 68(1)**	1440.781 67(2)[144] 1440.781 70(5)[10] 1440.781 5(1)[143] 1440.781(1)[169]
1541.967	$(0\,0\,0)6_{3,3} \leftarrow (0\,0\,0)5_{4,2}$	**1541.967 02(1)**	1541.966 98(5)[10] 1541.967 01(8)[145] 1541.966 8(2)[143]
1602.219	$(0\,0\,0)4_{1,3} \leftarrow (0\,0\,0)4_{0,4}$	**1602.219 237(8)**	1602.219 18(7)[143] 1602.219 2(1)[144] 1602.219 4(1)[145]
1661.008	$(0\,0\,0)2_{2,1} \leftarrow (0\,0\,0)2_{1,2}$	**1661.007 734(4)**	1661.007 73(5)[10] 1661.007 6(1)[143]
1669.905	$(0\,0\,0)2_{1,2} \leftarrow (0\,0\,0)1_{0,1}$	**1669.904 805(3)**	1669.904 81(5)[10] 1669.904 78(7)[143]
1713.883	$(0\,0\,0)4_{3,2} \leftarrow (0\,0\,0)5_{0,5}$	**1713.883 00(1)**	1713.883 00(5)[10] 1713.882 97(7)[143]
1716.770	$(0\,0\,0)3_{0,3} \leftarrow (0\,0\,0)2_{1,2}$	**1716.769 691(4)**	1716.769 69(5)[10] 1716.769 63(7)[143]
1716.957	$(0\,0\,0)5_{3,3} \leftarrow (0\,0\,0)6_{0,6}$	**1716.956 811(3)**	1716.956 79(5)[10]
1762.043	$(0\,0\,0)6_{3,3} \leftarrow (0\,0\,0)6_{2,4}$	**1762.042 824(7)**	1762.042 81(5)[10] 1762.042 79(7)[143] 1762.042 5(5)[169]
1794.789	$(0\,0\,0)6_{2,4} \leftarrow (0\,0\,0)6_{1,5}$	**1794.788 968(7)**	1794.788 92(5)[10] 1794.788 95(7)[143]
1867.749	$(0\,0\,0)5_{3,2} \leftarrow (0\,0\,0)5_{2,3}$	**1867.748 645(6)**	1867.748 66(5)[10] 1867.748 59(7)[143] 1867.748 4(5)[169]
1880.753	$(0\,0\,0)6_{3,4} \leftarrow (0\,0\,0)7_{0,7}$	**1880.752 56(1)**	1880.752 60(5)[144]
1893.687	$(0\,0\,0)3_{3,1} \leftarrow (0\,0\,0)4_{0,4}$	**1893.686 482(8)**	1893.686 51(5)[144]
1918.485	$(0\,0\,0)5_{2,3} \leftarrow (0\,0\,0)4_{3,2}$	**1918.485 335(9)**	1918.485 33(5)[10] 1918.485 35(5)[144] 1918.485 32(7)[143]
1919.360	$(0\,0\,0)3_{2,2} \leftarrow (0\,0\,0)3_{1,3}$	**1919.359 452(6)**	1919.359 45(5)[10] 1919.359 53(7)[143]
2014.865	$(0\,0\,0)5_{4,2} \leftarrow (0\,0\,0)6_{1,5}$	**2014.864 772(9)**	2014.864 86(9)[10]
2040.477	$(0\,0\,0)4_{3,1} \leftarrow (0\,0\,0)4_{2,2}$	**2040.476 843(8)**	2040.476 81(7)[143] 2040.477 4(5)[169]

TABLE 3. (*Continued.*)

f(NASEM) (GHz)	$(v_1' v_2' v_3')J'_{K_a',K_c'} \leftarrow (v_1'' v_2'' v_3'')J''_{K_a''K_c''}$	*f*(xMARVEL) (GHz)	*f*(expt.) (GHz)
2074.432	$(0\,0\,0)4_{1,3} \leftarrow (0\,0\,0)3_{2,2}$	**2074.432 386(9)**	2074.432 31(8)[143]
2164.132	$(0\,0\,0)3_{1,3} \leftarrow (0\,0\,0)2_{0,2}$	**2164.131 933(6)**	2164.131 98(7)[143]
2196.346	$(0\,0\,0)3_{3,0} \leftarrow (0\,0\,0)3_{2,1}$	**2196.345 80(1)**	2196.345 76(7)[143]
2221.751	$(0\,0\,0)5_{1,4} \leftarrow (0\,0\,0)5_{0,5}$	**2221.750 30(1)**	2221.750 5(2)[143] 2221.749 6(6)[169]
2264.150	$(0\,0\,0)4_{2,3} \leftarrow (0\,0\,0)4_{1,4}$	**2264.149 52(1)**	2264.149 7(1)[143] 2264.149 9(5)[169]
2344.290	$(0\,0\,0)7_{2,5} \leftarrow (0\,0\,0)7_{1,6}$	**2344.250 438(9)**	2344.250 3(1)[143]
2365.900	$(0\,0\,0)3_{3,1} \leftarrow (0\,0\,0)3_{2,2}$	**2365.899 631(9)**	2365.899 66(7)[143]
2391.573	$(0\,0\,0)4_{0,4} \leftarrow (0\,0\,0)3_{1,3}$	**2391.572 601(3)**	2391.572 63(7)[143]
2462.933	$(0\,0\,0)4_{3,2} \leftarrow (0\,0\,0)4_{2,3}$	**2462.933 059(7)**	2462.933 03(7)[143]
2630.960	$(0\,0\,0)5_{3,3} \leftarrow (0\,0\,0)5_{2,4}$	**2630.959 501(7)**	2630.959 52(7)[143] 2630.959 6(1)[70]
2640.474	$(0\,0\,0)4_{1,4} \leftarrow (0\,0\,0)3_{0,3}$	**2640.473 829(6)**	2640.473 84(7)[143] 2640.473 8(1)[70]
2657.666	$(0\,0\,0)4_{4,1} \leftarrow (0\,0\,0)5_{1,4}$	**2657.665 723(8)**	2657.665 79(7)[139] 2657.665 8(1)[70]
2664.561	$(0\,0\,0)7_{4,3} \leftarrow (0\,0\,0)7_{3,4}$	**2664.570 68(1)**	2664.570 70(7)[143] 2664.570 8(1)[70]
2685.639	$(0\,0\,0)5_{2,4} \leftarrow (0\,0\,0)5_{1,5}$	**2685.638 988(8)**	2685.638 97(7)[143] 2685.639 0(1)[70]
2773.977	$(0\,0\,0)2_{2,1} \leftarrow (0\,0\,0)1_{1,0}$	**2773.976 551(2)**	2773.976 59(7)[143]
2880.025	$(0\,0\,0)6_{3,4} \leftarrow (0\,0\,0)6_{2,5}$	**2880.025 39(1)**	2880.025 37(7)[143] 2880.025 2(5)[169]
2884.279	$(0\,0\,0)6_{1,5} \leftarrow (0\,0\,0)6_{0,6}$	**2884.278 944(6)**	2884.278 94(7)[143]
2884.941	$(0\,0\,0)6_{4,2} \leftarrow (0\,0\,0)6_{3,3}$	**2884.941 05(1)**	2884.941 05(7)[143]
2962.111	$(0\,0\,0)6_{2,4} \leftarrow (0\,0\,0)5_{3,3}$	**2962.111 101(4)**	2962.111 09(7)[143]
2968.749	$(0\,0\,0)2_{2,0} \leftarrow (0\,0\,0)1_{1,1}$	**2968.748 638(6)**	2968.748 65(7)[143]
2970.800	$(0\,0\,0)5_{1,4} \leftarrow (0\,0\,0)4_{2,3}$	**2970.800 360(7)**	2970.800 2(1)[143]

[a] *f*(NASEM), *f*(xMARVEL), and *f*(expt.) denote the estimated, the xMARVEL-predicted, and the experimental frequency of the $(v_1' v_2' v_3')J'_{K_a',K_c'} \leftarrow (v_1'' v_2'' v_3'')J''_{K_a''K_c''}$ line, respectively (the latter two values with the uncertainties of their last few digits). A factor of 100, compared to the uncertainties of the xMARVEL-predicted frequencies, is used as a cutoff for reporting W2020 entries in this table. The *f*(expt.) values of multiple measurements follow the order of their increased uncertainties. Where the xMARVEL predictions have smaller uncertainties than the most accurate literature observations, the corresponding values are highlighted in boldface. All transitions belong to the ground vibrational state.

and Medicine,[230] the W2020 database contains several sources reporting transitions with an accuracy of 10 kHz or better. It is expected that more and more such highly accurate transitions will become available in the near future for water isotopologues and beyond.

Recent studies reporting highly accurate data for $H_2{}^{16}O$ are 20ToFuSiCs,[44] 18KaStCaDa,[29] and 18ChHuTaSu[26] with uncertainties of about 2×10^{-7}, 4×10^{-7}, and 8×10^{-7} cm^{-1}, respectively. While 18KaStCaDa[29] and 18ChHuTaSu[26] recorded only a few ultraprecise lines, 20ToFuSiCs[44] published 156 extremely accurate transitions in the near infrared, leading (by design) to benchmark energy levels within the vibrational ground state and those corresponding to the $P = 4$ and $P = 5$ polyad. Consequently, the uncertainties of most of the (0 0 0) rotational levels of $H_2{}^{16}O$ with $J \leq 8$ are lowered in W2020 by about two orders of magnitude compared to those of Part III.

As to the data in Table 3, we note that there exists a regularly updated extended catalog of frequency allocations and spectrum protection for scientific uses.[230] This catalog is important for astronomical applications and includes a number of $H_2{}^{16}O$ lines, with the approximate rest frequencies and assignments recalled in Table 3. For all these protected $H_2{}^{16}O$ frequencies, several independent, highly accurate experimental determinations are available (see the last column of Table 3); all are included in the W2020 database. However, due to the efforts of Ref. 44, the protected transition frequencies can often be obtained more accurately from xMARVEL-based predictions than from direct, in fact, less precise, THz observations (see the fourth column of Table 3). Overall, the W2020 frequencies listed in the third column of Table 3 are the most accurate estimates of the rest frequencies of certain rotational lines of $H_2{}^{16}O$ under protection, important for a number of scientific and engineering applications.

5. Summary and Conclusions

After the latest improvements associated with the MARVEL protocol,[87,106] in particular, the introduction of the extMARVEL scheme[87] and the XML-based data management developed during the present study, as well as after learning about the large number of new

(ultra)high-precision spectroscopic studies on $H_2{}^{16}O$, we started a project aimed at the revision of the $H_2{}^{16}O$ database published by an IUPAC TG in 2013.[3] The XML-based line-by-line data treatment devised during this study helps to improve how we store, share, and transport spectroscopic data. Our XML-based input helps to (a) maintain the provenance of the data, (b) have a timestamp on the individual MARVEL entries, and (c) maintain a description of the "original" literature source and its data. It is planned that in the future, all MARVEL-based studies will utilize the considerable advantages of the XML format. To distinguish the new protocol from the old one, we use the name xMARVEL for the improved technique and code. Utilizing xMARVEL, revision and significant extension of the IUPAC Part III database[3] was achieved in several steps.

First, we collected all sources published after 2013 and checked the literature for sources missed during the compilation of the IUPAC Part III database. Due to this extensive search, 78 new experimental sources were added to the Part III dataset of $H_2{}^{16}O$ rovibrational transitions and two sources (81Kyro[110] and 05ZoShPoTe[111]) were permanently deleted from it. The new sources contain a large number of new and/or remeasured transitions, and they result in about 800 new empirical energy levels. In total, the new W2020 database of $H_2{}^{16}O$ contains 267 289 validated transitions that yield 19 204 rovibrational energy values with dependable, statistically significant uncertainties.

Second, we "optimized" the uncertainties of the observed lines. The aim of what we call optimization has been to decrease the uncertainties as much as possible within the experimental limitations, including occasional recalibration. These optimized uncertainties are used to classify the recorded transitions of a given source into segments, as required by the extMARVEL protocol. Note that extMARVEL was designed to retain the accuracy of the most precise experiments during the MARVEL analysis and transfer that to the energy values. This means that a large number of the empirical energy levels of this study have uncertainties characteristic of the high-precision measurements considered during the construction of the W2020 database. This also implies that some of these transitions surpass the accuracy of those maintained by the National Academies of Sciences, Engineering, and Medicine[230] and the International Astronomical Union, updating our previous related compilation.[87]

Third, we attempted to create the best set of self-consistent labels for the rovibrational energy levels. Occasionally, this meant modifications of some of the published labels. While recognizing that only the J quantum number and the parity of the state are unique descriptors, it is still felt that most of the labels of this study provide at least an approximate picture about the relevant rovibrational motions characterizing the quantum states of $H_2{}^{16}O$.

One must comment on the fact that, although the W2020 database contains significantly more entries than the IUPAC database, the number of energy levels these transitions determine is about the same in the two databases. This observation is in itself an important warning that high-resolution experiments should be designed much more efficiently if the goal is to extend our knowledge about the rovibrational states of $H_2{}^{16}O$. The number of empirical energy levels is still less than 20 000, which should be compared to the about one million bound rovibrational states of $H_2{}^{16}O$ indicated by the best first-principles computations.[31,93]

Construction of the W2020 database of the rovibrational transitions of $H_2{}^{16}O$ involved their in-depth validation. During this process, we compared the W2020 energies, obtained via the xMARVEL protocol, with first-principles (PoKaZaTeL[31] and BT2[109]) energy lists in order to check whether all the W2020 states can be matched with their theoretical counterparts within appropriate symmetry and J values. As a result of this comparison and due to some missing links, 229 energy levels had to be removed from the PCs. We also compared the W2020 energies with the previously published rovibrational datasets of $H_2{}^{16}O$ (01LaCoCa,[227] 04CoPiVeLa,[179] 14CoMaPi,[11] and JPL[228]), augmented with a thorough matching of the W2020 and Part III datasets. These tests show that the W2020 dataset not only better represents the original literature sources, but its empirical energy levels are more accurate and reliable than their Part III counterparts.

Finally, note that the much improved accuracy of the $J \leq 8$ rotational lines present in W2020, resulting mostly from the precision-spectroscopy measurements of Ref. 44, means that the upper energy levels deduced in several sources[8,26,173,231] reporting highly accurate transitions would change significantly. This secondary effect of the W2020 dataset must be taken into account in future studies.

6. Supplementary Material

See the supplementary material for listings of transitions and energy levels characterizing the W2020 dataset.

Acknowledgments

The work performed in Budapest received support from the NKFIH (Grant No. K119658), from the ELTE Excellence Program (Grant No. 1783-3/2018/FEKUTSTRAT) supported by the Hungarian Ministry of Human Capacities (EMMI), and from Grant No. VEKOP-2.3.2-16-2017-000. The work performed in the United Kingdom received support from the UK Natural Environment Research Council through grant NE/T000767/1. The joint work between the Budapest and London groups received support from the COST Action MOLIM (Molecules in Motion, CM1405) in the form of a Short Term Scientific Mission (STSM) awarded to A.G.C. Dr. Semen Mikhailenko is thanked for fruitful discussions.

7. Data Availability

The data that support the findings of this study are available within the article (and its supplementary material) and on the ReSpecTh website (http://ReSpecTh.hu).

8. References

[1]J. Tennyson, P. F. Bernath, L. R. Brown, A. Campargue, M. R. Carleer, A. G. Császár, R. R. Gamache, J. T. Hodges, A. Jenouvrier, O. V. Naumenko, O. L. Polyansky, L. S. Rothman, R. A. Toth, A. C. Vandaele, N. F. Zobov, L. Daumont, A. Z. Fazliev, T. Furtenbacher, I. E. Gordon, S. N. Mikhailenko, and S. V. Shirin, J. Quant. Spectrosc. Radiat. Transfer **110**, 573 (2009).

[2]J. Tennyson, P. F. Bernath, L. R. Brown, A. Campargue, A. G. Császár, L. Daumont, R. R. Gamache, J. T. Hodges, O. V. Naumenko, O. L. Polyansky, L. S. Rothman, R. A. Toth, A. C. Vandaele, N. F. Zobov, S. Fally, A. Z. Fazliev, T. Furtenbacher, I. E. Gordon, S.-M. Hu, S. N. Mikhailenko, and B. A. Voronin, J. Quant. Spectrosc. Radiat. Transfer **111**, 2160 (2010).

[3]J. Tennyson, P. F. Bernath, L. R. Brown, A. Campargue, M. R. Carleer, A. G. Császár, L. Daumont, R. R. Gamache, J. T. Hodges, O. V. Naumenko, O. L. Polyansky, L. S. Rothman, A. C. Vandaele, N. F. Zobov, A. R. Al Derzi, C. Fábri, A. Z. Fazliev, T. Furtenbacher, I. E. Gordon, L. Lodi, and I. I. Mizus, J. Quant. Spectrosc. Radiat. Transfer **117**, 29 (2013).
[4]J. Tennyson, P. F. Bernath, L. R. Brown, A. Campargue, A. G. Császár, L. Daumont, R. R. Gamache, J. T. Hodges, O. V. Naumenko, O. L. Polyansky, L. S. Rothman, A. C. Vandaele, N. F. Zobov, N. Dénes, A. Z. Fazliev, T. Furtenbacher, I. E. Gordon, S.-M. Hu, T. Szidarovszky, and I. A. Vasilenko, J. Quant. Spectrosc. Radiat. Transfer **142**, 93 (2014).
[5]J. Tennyson, P. F. Bernath, L. R. Brown, A. Campargue, A. G. Császár, L. Daumont, R. R. Gamache, J. T. Hodges, O. V. Naumenko, O. L. Polyansky, L. S. Rothman, A. C. Vandaele, and N. F. Zobov, Pure Appl. Chem. **86**, 71 (2014).
[6]G. Cazzoli and C. Puzzarini, J. Phys. Chem. A **117**, 13759 (2013).
[7]O. Leshchishina, S. N. Mikhailenko, D. Mondelain, S. Kassi, and A. Campargue, J. Quant. Spectrosc. Radiat. Transfer **130**, 69 (2013).
[8]Y. Lu, X.-F. Li, J. Wang, A.-W. Liu, and S.-M. Hu, J. Quant. Spectrosc. Radiat. Transfer **118**, 96 (2013).
[9]S. N. Mikhailenko, V. I. Serdyukov, L. N. Sinitsa, and S. S. Vasilchenko, Opt. Spectrosc. **115**, 912 (2013).
[10]S. Yu, J. C. Pearson, and B. J. Drouin, J. Mol. Spectrosc. **288**, 7 (2013).
[11]L. H. Coudert, M.-A. Martin-Drumel, and O. Pirali, J. Mol. Spectrosc. **303**, 36 (2014).
[12]A.-W. Liu, O. V. Naumenko, S. Kassi, and A. Campargue, J. Quant. Spectrosc. Radiat. Transfer **138**, 97 (2014).
[13]K. Y. Osipov, V. A. Kapitanov, A. E. Protasevich, A. A. Pereslavtseva, and Y. Y. Ponurovsky, J. Quant. Spectrosc. Radiat. Transfer **142**, 1 (2014).
[14]L. Regalia, C. Oudot, S. Mikhailenko, L. Wang, X. Thomas, A. Jenouvrier, and P. Von der Heyden, J. Quant. Spectrosc. Radiat. Transfer **136**, 119 (2014).
[15]L. N. Sinitsa, V. I. Serduykov, S. S. Vasilchenko, A. D. Bykov, A. P. Shcherbakov, E. R. Polovtseva, and K. V. Kalinin, in *20th International Symposium on Atmospheric and Ocean Optics: Atmospheric Physics*, edited by O. A. Romanovskii (SPIE, Bellingham, WA, 2014) article 92920J.
[16]A. Campargue, S. N. Mikhailenko, B. G. Lohan, E. V. Karlovets, D. Mondelain, and S. Kassi, J. Quant. Spectrosc. Radiat. Transfer **157**, 135 (2015).
[17]D. S. Makarov, M. A. Koshelev, N. F. Zobov, and O. V. Boyarkin, Chem. Phys. Lett. **627**, 73 (2015).
[18]G. C. Mellau, S. N. Mikhailenko, and V. G. Tyuterev, J. Mol. Spectrosc. **308-309**, 6 (2015).
[19]S. N. Mikhailenko, V. I. Serdyukov, and L. N. Sinitsa, J. Quant. Spectrosc. Radiat. Transfer **156**, 36 (2015).
[20]V. T. Sironneau and J. T. Hodges, J. Quant. Spectrosc. Radiat. Transfer **152**, 1 (2015).
[21]L. N. Sinitsa, V. I. Serdyukov, S. S. Vasil'chenko, A. D. Bykov, A. P. Shcherbakov, E. R. Polovtseva, and K. V. Kalinin, Opt. Spectrosc. **118**, 697 (2015).
[22]S. N. Mikhailenko, O. Leshchishina, E. V. Karlovets, D. Mondelain, S. Kassi, and A. Campargue, J. Quant. Spectrosc. Radiat. Transfer **177**, 108 (2016).
[23]M. Birk, G. Wagner, J. Loos, L. Lodi, O. L. Polyansky, A. A. Kyuberis, N. F. Zobov, and J. Tennyson, J. Quant. Spectrosc. Radiat. Transfer **203**, 88 (2017).
[24]J. Loos, M. Birk, and G. Wagner, J. Quant. Spectrosc. Radiat. Transfer. **203**, 119 (2017).
[25]D. Mondelain, S. N. Mikhailenko, E. V. Karlovets, S. Béguier, S. Kassi, and A. Campargue, J. Quant. Spectrosc. Radiat. Transfer **203**, 206 (2017).
[26]J. Chen, T.-P. Hua, L.-G. Tao, Y. R. Sun, A.-W. Liu, and S.-M. Hu, J. Quant. Spectrosc. Radiat. Transfer **205**, 91 (2018).
[27]E. Czinki, T. Furtenbacher, A. G. Császár, A. K. Eckhardt, and G. C. Mellau, J. Quant. Spectrosc. Radiat. Transfer **206**, 46 (2018).
[28]V. M. Devi, R. R. Gamache, B. Vispoel, C. L. Renaud, D. C. Benner, M. A. H. Smith, T. A. Blake, and R. L. Sams, J. Mol. Spectrosc. **348**, 13 (2018).
[29]S. Kassi, T. Stoltmann, M. Casado, M. Daëron, and A. Campargue, J. Chem. Phys. **148**, 054201 (2018).
[30]S. N. Mikhailenko, V. I. Serdyukov, and L. N. Sinitsa, J. Quant. Spectrosc. Radiat. Transfer **217**, 170 (2018).
[31]O. L. Polyansky, A. A. Kyuberis, N. F. Zobov, J. Tennyson, S. N. Yurchenko, and L. Lodi, Mon. Not. R. Astron. Soc. **480**, 2597 (2018).
[32]L. Rutkowski, A. Foltynowicz, F. M. Schmidt, A. C. Johansson, A. Khodabakhsh, A. A. Kyuberis, N. F. Zobov, O. L. Polyansky, S. N. Yurchenko, and J. Tennyson, J. Quant. Spectrosc. Radiat. Transfer **205**, 213 (2018).
[33]P. J. Schroeder, M. J. Cich, J. Yang, F. R. Giorgetta, W. C. Swann, I. Coddington, N. R. Newbury, B. J. Drouin, and G. B. Rieker, J. Quant. Spectrosc. Radiat. Transfer **210**, 240 (2018).
[34]L. N. Sinitsa, V. I. Serdyukov, E. R. Polovtseva, A. D. Bykov, and A. P. Shcherbakov, Atmos. Oceanic Opt. **31**, 329 (2018).
[35]V. I. Serdyukov, L. N. Sinitsa, S. S. Vasilchenko, N. N. Lavrentieva, A. S. Dudaryonok, and A. P. Scherbakov, J. Quant. Spectrosc. Radiat. Transfer **219**, 213 (2018).
[36]Y. Tan, S. N. Mikhailenko, J. Wang, A.-W. Liu, X.-Q. Zhao, G.-L. Liu, and S.-M. Hu, J. Quant. Spectrosc. Radiat. Transfer **221**, 233 (2018).
[37]A.-W. Liu, G.-L. Liu, X.-Q. Zhao, J. Wang, Y. Tan, and S.-M. Hu, J. Quant. Spectrosc. Radiat. Transfer **239**, 106651 (2019).
[38]S. N. Mikhailenko, E. V. Karlovets, S. Vasilchenko, D. Mondelain, S. Kassi, and A. Campargue, J. Quant. Spectrosc. Radiat. Transfer **236**, 106574 (2019).
[39]S. N. Mikhailenko, D. Mondelain, E. V. Karlovets, S. Kassi, and A. Campargue, J. Quant. Spectrosc. Radiat. Transfer **222-223**, 229 (2019).
[40]L. Régalia, X. Thomas, T. Rennesson, and S. Mikhailenko, J. Quant. Spectrosc. Radiat. Transfer **235**, 257 (2019).
[41]V. I. Serdyukov, L. N. Sinitsa, N. N. Lavrentieva, and A. S. Dudaryonok, J. Quant. Spectrosc. Radiat. Transfer **234**, 47 (2019).
[42]S. Vasilchenko, H. Tran, D. Mondelain, S. Kassi, and A. Campargue, J. Quant. Spectrosc. Radiat. Transfer **235**, 332 (2019).
[43]A. Campargue, S. Kassi, A. Yachmenev, A. A. Kyuberis, J. Küpper, and S. N. Yurchenko, Phys. Rev. Res. **2**, 023091 (2020).
[44]R. Tóbiás, T. Furtenbacher, I. Simkó, A. G. Császár, M. L. Diouf, F. M. J. Cozijn, J. M. A. Staa, E. J. Salumbides, and W. Ubachs, Nat. Commun. **11**, 1708 (2020).
[45]R. T. Hall and J. M. Dowling, J. Chem. Phys. **47**, 2454 (1967).
[46]W. S. Benedict, M. A. Pollack, and W. J. Tomlinson III, IEEE J. Quantum. Electron. **5**, 108 (1969).
[47]P. E. Fraley and K. Narahari Rao, J. Mol. Spectrosc. **29**, 348 (1969).
[48]K. M. Evenson, J. S. Wells, L. M. Matarrese, and L. B. Elwell, Appl. Phys. Lett. **16**, 159 (1970).
[49]D. A. Stephenson and R. G. Strauch, J. Mol. Spectrosc. **35**, 494 (1970).
[50]J.-M. Flaud, C. Camy-Peyret, and J. P. Maillard, Mol. Phys. **32**, 499 (1976).
[51]J. W. Fleming and M. J. Gibson, J. Mol. Spectrosc. **62**, 326 (1976).
[52]T. D. Wilkerson, G. Schwemmer, B. Gentry, and L. P. Giver, J. Quant. Spectrosc. Radiat. Transfer **22**, 315 (1979).
[53]J. Kauppinen and E. Kyrö, J. Mol. Spectrosc. **84**, 405 (1980).
[54]R. A. Toth and J. W. Brault, Appl. Opt. **22**, 908 (1983).
[55]J.-Y. Mandin, J.-P. Chevillard, C. Camy-Peyret, and J.-M. Flaud, J. Mol. Spectrosc. **116**, 167 (1986).
[56]V. N. Markov and A. F. Krupnov, J. Mol. Spectrosc. **172**, 211 (1995).
[57]L. R. Brown and C. Plymate, J. Quant. Spectrosc. Radiat. Transfer **56**, 263 (1996).
[58]A. Bauer, M. Godon, J. Carlier, and R. R. Gamache, J. Quant. Spectrosc. Radiat. Transfer **59**, 273 (1998).
[59]*Seventh International Symposium on Atmospheric and Ocean Optics*, edited by G. G. Matvienko and M. V. Panchenko (SPIE, Tomsk, Russian federation, 2000), Vol. 4341.
[60]N. F. Zobov, O. L. Polyansky, J. Tennyson, S. V. Shirin, R. Nassar, T. Hirao, T. Imajo, P. F. Bernath, and L. Wallace, Astrophys. J. **530**, 994 (2000).
[61]R. Schermaul, R. C. M. Learner, A. A. D. Canas, J. W. Brault, O. L. Polyansky, D. Belmiloud, N. F. Zobov, and J. Tennyson, J. Mol. Spectrosc. **211**, 169 (2002).
[62]R. N. Tolchenov, J. Tennyson, S. V. Shirin, N. F. Zobov, O. L. Polyansky, and A. N. Maurellis, J. Mol. Spectrosc. **221**, 99 (2003).
[63]Q. Zou and P. Varanasi, J. Quant. Spectrosc. Radiat. Transfer **82**, 45 (2003).
[64]S. V. Shirin, N. F. Zobov, O. L. Polyansky, J. Tennyson, T. Parekunnel, and P. F. Bernath, J. Chem. Phys. **120**, 206 (2004).
[65]G. Y. Golubiatnikov, J. Mol. Spectrosc. **230**, 196 (2005).

[66]I. V. Ptashnik, K. M. Smith, and K. P. Shine, J. Mol. Spectrosc. **232**, 186 (2005).
[67]N. F. Zobov, R. I. Ovsannikov, S. V. Shirin, O. L. Polyansky, J. Tennyson, A. Janka, and P. F. Bernath, J. Mol. Spectrosc. **240**, 112 (2006).
[68]F. Mazzotti, R. N. Tolchenov, and A. Campargue, J. Mol. Spectrosc. **243**, 78 (2007).
[69]M. D. De Vizia, F. Rohart, A. Castrillo, E. Fasci, L. Moretti, and L. Gianfrani, Phys. Rev. A **83**, 052506 (2011).
[70]B. J. Drouin, S. Yu, J. C. Pearson, and H. Gupta, J. Mol. Struct. **1006**, 2 (2011).
[71]G. Galzerano, A. Gambetta, E. Fasci, A. Castrillo, M. Marangoni, P. Laporta, and L. Gianfrani, Appl. Phys. B **102**, 725 (2011).
[72]M. A. Koshelev, J. Quant. Spectrosc. Radiat. Transfer **112**, 550 (2011).
[73]O. M. Leshchishina, O. V. Naumenko, and A. Campargue, J. Mol. Spectrosc. **268**, 28 (2011).
[74]O. M. Leshchishina, O. V. Naumenko, and A. Campargue, J. Quant. Spectrosc. Radiat. Transfer **112**, 913 (2011).
[75]A.-W. Liu, K.-F. Song, H.-Y. Ni, S.-M. Hu, O. V. Naumenko, I. A. Vasilenko, and S. N. Mikhailenko, J. Mol. Spectrosc. **265**, 26 (2011).
[76]S. Mikhailenko, S. Kassi, L. Wang, and A. Campargue, J. Mol. Spectrosc. **269**, 92 (2011).
[77]L. Daumont, A. Jenouvrier, S. Mikhailenko, M. Carleer, C. Hermans, S. Fally, and A. C. Vandaele, J. Quant. Spectrosc. Radiat. Transfer **113**, 878 (2012).
[78]M. J. Down, J. Tennyson, J. Orphal, P. Chelin, and A. A. Ruth, J. Mol. Spectrosc. **282**, 1 (2012).
[79]O. Leshchishina, S. Mikhailenko, D. Mondelain, S. Kassi, and A. Campargue, J. Quant. Spectrosc. Radiat. Transfer **113**, 2155 (2012).
[80]S. N. Mikhailenko, O. V. Naumenko, A. V. Nikitin, I. A. Vasilenko, A.-W. Liu, K.-F. Song, H.-Y. Ni, and S.-M. Hu, J. Quant. Spectrosc. Radiat. Transfer **113**, 653 (2012).
[81]C. Oudot, L. Régalia, S. Mikhailenko, X. Thomas, P. Von Der Heyden, and D. Décatoire, J. Quant. Spectrosc. Radiat. Transfer **113**, 859 (2012).
[82]C. Puzzarini, G. Cazzoli, and J. Gauss, J. Chem. Phys. **137**, 154311 (2012).
[83]S. S. Vasilchenko, S. N. Mikhailenko, V. I. Serdyukov, and L. N. Sinitsa, Opt. Spectrosc. **113**, 451–455 (2012).
[84]J. Tennyson, N. F. Zobov, R. Williamson, O. L. Polyansky, and P. F. Bernath, J. Phys. Chem. Ref. Data **30**, 735 (2001).
[85]T. Furtenbacher, A. G. Császár, and J. Tennyson, J. Mol. Spectrosc. **245**, 115 (2007).
[86]T. Furtenbacher and A. G. Császár, J. Quant. Spectrosc. Radiat. Transfer **113**, 929 (2012).
[87]R. Tóbiás, T. Furtenbacher, J. Tennyson, and A. G. Császár, Phys. Chem. Chem. Phys. **21**, 3473 (2019).
[88]I. E. Gordon, L. S. Rothman, C. Hill, R. V. Kochanov, Y. Tan, P. F. Bernath, M. Birk, V. Boudon, A. Campargue, K. V. Chance, B. J. Drouin, J.-M. Flaud, R. R. Gamache, J. T. Hodges, D. Jacquemart, V. I. Perevalov, A. Perrin, K. P. Shine, M.-A. H. Smith, J. Tennyson, G. C. Toon, H. Tran, V. G. Tyuterev, A. Barbe, A. G. Császár, V. M. Devi, T. Furtenbacher, J. J. Harrison, J.-M. Hartmann, A. Jolly, T. J. Johnson, T. Karman, I. Kleiner, A. A. Kyuberis, J. Loos, O. M. Lyulin, S. T. Massie, S. N. Mikhailenko, N. Moazzen-Ahmadi, H. S. P. Müller, O. V. Naumenko, A. V. Nikitin, O. L. Polyansky, M. Rey, M. Rotger, S. W. Sharpe, K. Sung, E. Starikova, S. A. Tashkun, J. V. Auwera, G. Wagner, J. Wilzewski, P. Wcisło, S. Yu, and E. J. Zak, J. Quant. Spectrosc. Radiat. Transfer **203**, 3 (2017).
[89]N. N. Lavrentieva, B. A. Voronin, O. V. Naumenko, A. D. Bykov, and A. A. Fedorova, Icarus **236**, 38 (2014).
[90]A. A. Kyuberis, N. F. Zobov, O. V. Naumenko, B. A. Voronin, O. L. Polyansky, L. Lodi, A. Liu, S.-M. Hu, and J. Tennyson, J. Quant. Spectrosc. Radiat. Transfer **203**, 175 (2017).
[91]N. Jacquinet-Husson, R. Armante, N. A. Scott, A. Chédin, L. Crépeau, C. Boutammine, A. Bouhdaoui, C. Crevoisier, V. Capelle, C. Boonne, N. Poulet-Crovisier, A. Barbe, D. Chris Benner, V. Boudon, L. R. Brown, J. Buldyreva, A. Campargue, L. H. Coudert, V. M. Devi, M. J. Down, B. J. Drouin, A. Fayt, C. Fittschen, J.-M. Flaud, R. R. Gamache, J. J. Harrison, C. Hill, Ø. Hodnebrog, S.-M. Hu, D. Jacquemart, A. Jolly, E. Jiménez, N. N. Lavrentieva, A.-W. Liu, L. Lodi, O. M. Lyulin, S. T. Massie, S. Mikhailenko, H. S. P. Müller, O. V. Naumenko, A. Nikitin, C. J. Nielsen, J. Orphal, V. I. Perevalov, A. Perrin, E. Polovtseva, A. Predoi-Cross, M. Rotger, A. A. Ruth, S. S. Yu, K. Sung, S. A. Tashkun, J. Tennyson, V. G. Tyuterev, J. Vander Auwera, B. A. Voronin, and A. Makie, J. Mol. Spectrosc. **327**, 31 (2016).
[92]O. L. Polyansky, A. A. Kyuberis, L. Lodi, J. Tennyson, S. N. Yurchenko, R. I. Ovsyannikov, and N. F. Zobov, Mon. Not. R. Astron. Soc. **466**, 1363 (2017).
[93]T. Furtenbacher, T. Szidarovszky, J. Hrubý, A. A. Kyuberis, N. F. Zobov, O. L. Polyansky, J. Tennyson, and A. G. Császár, J. Phys. Chem. Ref. Data **45**, 043104 (2016).
[94]I. Simkó, T. Furtenbacher, J. Hrubý, N. F. Zobov, O. L. Polyansky, J. Tennyson, R. R. Gamache, T. Szidarovszky, N. Dénes, and A. G. Császár, J. Phys. Chem. Ref. Data **46**, 023104 (2017).
[95]R. R. Gamache, C. Roller, E. Lopes, I. E. Gordon, L. S. Rothman, O. L. Polyansky, N. F. Zobov, A. A. Kyuberis, J. Tennyson, S. N. Yurchenko, A. G. Császár, T. Furtenbacher, X. Huang, D. W. Schwenke, T. J. Lee, B. J. Drouin, S. A. Tashkun, V. I. Perevalov, and R. V. Kochanov, J. Quant. Spectrosc. Radiat. Transfer **203**, 70 (2017).
[96]S. V. Shirin, O. L. Polyansky, N. F. Zobov, R. I. Ovsyannikov, A. G. Császár, and J. Tennyson, J. Mol. Spectrosc. **236**, 216 (2006).
[97]O. L. Polyansky, R. I. Ovsyannikov, A. A. Kyuberis, L. Lodi, J. Tennyson, and N. F. Zobov, J. Phys. Chem. A **117**, 9633–9643 (2013).
[98]T. Szidarovszky and A. G. Császár, Mol. Phys. **111**, 2131 (2013).
[99]I. I. Mizus, A. A. Kyuberis, N. F. Zobov, V. Y. Makhnev, O. L. Polyansky, and J. Tennyson, Philos. Trans. R. Soc. A **376**, 20170149 (2018).
[100]M. S. Child, T. Weston, and J. Tennyson, Mol. Phys. **96**, 371 (1999).
[101]A. Miani and J. Tennyson, J. Chem. Phys. **120**, 2732 (2004).
[102]T. Furtenbacher and A. G. Császár, J. Quant. Spectrosc. Radiat. Transfer **109**, 1234 (2008).
[103]A. G. Császár and T. Furtenbacher, J. Mol. Spectrosc. **266**, 99 (2011).
[104]A. G. Császár, T. Furtenbacher, and P. Árendás, J. Phys. Chem. A **120**, 8949 (2016).
[105]T. Furtenbacher, P. Árendás, G. Mellau, and A. G. Császár, Sci. Rep. **4**, 4654 (2014).
[106]R. Tóbiás, T. Furtenbacher, and A. G. Császár, J. Quant. Spectrosc. Radiat. Transfer **203**, 557 (2017).
[107]D. Darby-Lewis, H. Shah, D. Joshi, F. Khan, M. Kauwo, N. Sethi, P. F. Bernath, T. Furtenbacher, R. Tóbiás, A. G. Császár *et al.*, J. Mol. Spectrosc. **362**, 69 (2019).
[108]J. Tennyson, T. Furtenbacher, R. Tóbiás, and A. G. Császár, "xMARVEL" J. Quant. Spectrosc. Radiat. Transfer (unpublished) (2020).
[109]R. J. Barber, J. Tennyson, G. J. Harris, and R. N. Tolchenov, Mon. Not. R. Astron. Soc. **368**, 1087 (2006).
[110]E. Kyrö, J. Mol. Spectrosc. **88**, 167 (1981).
[111]N. F. Zobov, S. V. Shirin, O. L. Polyansky, J. Tennyson, P.-F. Coheur, P. F. Bernath, M. Carleer, and R. Colin, Chem. Phys. Lett. **414**, 193 (2005).
[112]F. Matsushima, N. Tomatsu, T. Nagai, Y. Moriwaki, and K. Takagi, J. Mol. Spectrosc. **235**, 190 (2006).
[113]L. R. Brown and R. A. Toth, J. Opt. Soc. Am. B **2**, 842 (1985).
[114]R. A. Toth, J. Quant. Spectrosc. Radiat. Transfer **94**, 51 (2005).
[115]R. A. Toth, J. Mol. Spectrosc. **194**, 28 (1999).
[116]N. F. Zobov, S. V. Shirin, R. I. Ovsyannikov, O. L. Polyansky, R. J. Barber, J. Tennyson, P. F. Bernath, M. Carleer, R. Colin, and P.-F. Coheur, Mon. Not. R. Astron. Soc. **387**, 1093 (2008).
[117]R. S. Mulliken, J. Chem. Phys. **23**, 1997 (1955).
[118]H. W. Kroto, *Molecular Rotation Spectra* (Dover, New York, 1992).
[119]M. Grechko, P. Maksyutenko, N. F. Zobov, S. V. Shirin, O. L. Polyansky, T. R. Rizzo, and O. V. Boyarkin, J. Phys. Chem. A **112**, 10539 (2008).
[120]M. Grechko, O. V. Boyarkin, T. R. Rizzo, P. Maksyutenko, N. F. Zobov, S. V. Shirin, L. Lodi, J. Tennyson, A. G. Császár, and O. L. Polyansky, J. Chem. Phys. **131**, 221105 (2009).
[121]G. Guelachvili and N. Picqué, in *Molecular Constants Mostly From Infrared Spectroscopy*, edited by G. Guelachvili (Springer, New York, NY, 2016), pp. 1–58.
[122]O. V. Boyarkin (private communication, 2020).
[123]A. G. Császár, W. D. Allen, and H. F. Schaefer III, J. Chem. Phys. **108**, 9751 (1998).
[124]G. Tarczay, A. G. Császár, W. Klopper, V. Szalay, W. D. Allen, and H. F. Schaefer III, J. Chem. Phys. **110**, 11971 (1999).

[125]E. F. Valeev, W. D. Allen, H. F. Schaefer III, and A. G. Császár, J. Chem. Phys. **114**, 2875 (2001).
[126]S. G. Kukolich, J. Chem. Phys. **50**, 3751 (1969).
[127]G. Cazzoli, C. Puzzarini, M. E. Harding, and J. Gauss, Chem. Phys. Lett. **473**, 21 (2009).
[128]C. Huiszoon, Rev. Sci. Instrum. **42**, 477 (1971).
[129]G. Y. Golubiatnikov, V. N. Markov, A. Guarnieri, and R. Knochel, J. Mol. Spectrosc. **240**, 251 (2006).
[130]M. A. Koshelev, M. Y. Tretyakov, G. Y. Golubiatnikov, V. V. Parshin, V. N. Markov, and I. A. Koval, J. Mol. Spectrosc. **241**, 101 (2007).
[131]M. Y. Tretyakov, M. A. Koshelev, I. N. Vilkov, V. V. Parshin, and E. A. Serov, J. Quant. Spectrosc. Radiat. Transfer **114**, 109 (2013).
[132]A. Bauer, M. Godon, M. Kheddar, and J. M. Hartmann, J. Quant. Spectrosc. Radiat. Transfer **41**, 49 (1989).
[133]G. Steenbeckeliers and J. Bellet, C. R. Acad. Sc. Paris **273**, 471 (1971).
[134]T. G. Blaney, C. C. Bradley, G. J. Edwards, and D. J. E. Knight, Phys. Lett. A **43**, 471 (1973).
[135]P. Helminger, J. K. Messer, and F. C. De Lucia, Appl. Phys. Lett. **42**, 309 (1983).
[136]J. K. Messer, F. C. De Lucia, and P. Helminger, Int. J. Infrared Millimeter Waves **4**, 505 (1983).
[137]H. Kuze, Astrophys. J. **239**, 1131 (1980).
[138]S. Golden, T. Wentink, R. Hillger, and M. W. P. Strandberg, Phys. Rev. **73**, 92 (1948).
[139]K. V. Chance, K. Park, and K. M. Evenson, J. Quant. Spectrosc. Radiat. Transfer **59**, 687 (1998).
[140]O. I. Baskakov, V. A. Alekseev, E. A. Alekseev, and B. I. Polevoi, Opt. Spectrosc. **63**, 1016 (1987).
[141]T. Amano and F. Scappini, Chem. Phys. Lett. **182**, 93 (1991).
[142]P. D. Natale, L. Lorini, M. Inguscio, I. G. Nolt, J. H. Park, G. D. Lonardo, L. Fusina, P. A. R. Ade, and A. G. Murray, Appl. Opt. **36**, 8526 (1997).
[143]F. Matsushima, H. Odashima, T. Iwasaki, S. Tsunekawa, and K. Takagi, J. Mol. Spectrosc. **352-353**, 371 (1995).
[144]S. Yu, J. C. Pearson, B. J. Drouin, M.-A. Martin-Drumel, O. Pirali, M. Vervloet, L. H. Coudert, H. S. P. Müller, and S. Brünken, J. Mol. Spectrosc. **279**, 16 (2012).
[145]G. Cazzoli, C. Puzzarini, G. Buffa, and O. Tarrini, J. Quant. Spectrosc. Radiat. Transfer **110**, 609 (2009).
[146]A. V. Burenin, T. M. Fevral'skikh, E. N. Karyakin, O. L. Polyansky, and S. M. Shapin, J. Mol. Spectrosc. **100**, 182 (1983).
[147]J. C. Pearson, T. Anderson, E. Herbst, F. C. De Lucia, and P. Helminger, Astrophys. J. **379**, L41 (1991).
[148]F. C. De Lucia, P. Helminger, R. L. Cook, and W. Gordy, Phys. Rev. A **5**, 487 (1972).
[149]J. C. Pearson, Ph.D. thesis, Duke University, Durham, NC, 1995.
[150]P. Chen, J. C. Pearson, H. M. Pickett, S. Matsuura, and G. A. Blake, Astrophys. J. Suppl. Ser. **128**, 371 (2000).
[151]M. Herman, J. W. C. Johns, and A. R. W. McKellar, Can. J. Phys. **57**, 397 (1979).
[152]C. K. Jen, Phys. Rev. **81**, 197 (1951).
[153]J.-M. Flaud, C. Camy-Peyret, and A. Valentin, J. Phys. **33**, 741 (1972).
[154]L. Joly, B. Parvitte, V. Zéninari, D. Courtois, and G. Durry, J. Quant. Spectrosc. Radiat. Transfer **102**, 129 (2006).
[155]V.-M. Horneman, R. Anttila, S. Alanko, and J. Pietilä, J. Mol. Spectrosc. **234**, 238 (2005).
[156]S. P. Belov, I. N. Kozin, O. L. Polyansky, M. Y. Tret'yakov, and N. F. Zobov, J. Mol. Spectrosc. **126**, 113 (1987).
[157]S. P. Belov (private communication, data from Ref. 150, 1996).
[158]W. C. King and W. Gordy, Phys. Rev. **93**, 407 (1954).
[159]G. Guelachvili, J. Opt. Soc. Am. **73**, 137 (1983).
[160]L. R. Brown and J. S. Margolis, J. Quant. Spectrosc. Radiat. Transfer **56**, 283 (1996).
[161]R. A. Toth, J. Opt. Soc. Am. B **8**, 2236 (1991).
[162]S. N. Mikhailenko, V. G. Tyuterev, K. A. Keppler, B. P. Winnewisser, M. Winnewisser, G. Mellau, S. Klee, and K. N. Rao, J. Mol. Spectrosc. **184**, 330 (1997).
[163]R. Paso and V.-M. Horneman, J. Opt. Soc. Am. B **12**, 1813 (1995).
[164]R. A. Toth, J. Opt. Soc. Am. B **10**, 1526 (1993).
[165]R. A. Toth, J. Opt. Soc. Am. B **10**, 2006 (1993).
[166]J. Kauppinen, K. Jolma, and V.-M. Horneman, Appl. Opt. **21**, 3332 (1982).
[167]R. A. Toth, Appl. Opt. **33**, 4851 (1994).
[168]S. N. Mikhailenko, D. Mondelain, E. V. Karlovets, S. Kassi, and A. Campargue, J. Quant. Spectrosc. Radiat. Transfer **206**, 163 (2018).
[169]J. W. C. Johns, J. Opt. Soc. Am. B **2**, 1340 (1985).
[170]G. Guelachvili and K. N. Rao, *Handbook of Infrared Standards* (Academic Press, Orlando, FL, USA, 1986).
[171]R. A. Toth, J. Mol. Spectrosc. **166**, 176 (1994).
[172]S. N. Mikhailenko, K. A. Keppler Albert, G. Mellau, S. Klee, B. P. Winnewisser, M. Winnewisser, and V. G. Tyuterev, J. Quant. Spectrosc. Radiat. Transfer **109**, 2687 (2008).
[173]S.-M. Hu, B. Chen, Y. Tan, J. Wang, C.-F. Cheng, and A.-W. Liu, J. Quant. Spectrosc. Radiat. Transfer **164**, 37 (2015).
[174]C. Camy-Peyret, J. M. Flaud, G. Guelachvili, and C. Amiot, Mol. Phys. **26**, 825 (1973).
[175]A. Jenouvrier, L. Daumont, L. Régalia-Jarlot, V. G. Tyuterev, M. Carleer, A. C. Vandaele, S. Mikhailenko, and S. Fally, J. Quant. Spectrosc. Radiat. Transfer **105**, 326 (2007).
[176]R. H. Partridge, J. Mol. Spectrosc. **87**, 429 (1981).
[177]S. N. Mikhailenko, W. Le, S. Kassi, and A. Campargue, J. Mol. Spectrosc. **244**, 170 (2007).
[178]A. S. Pine, M. J. Coulombe, C. Camy-Peyret, and J. M. Flaud, J. Phys. Chem. Ref. Data **12**, 413 (1983).
[179]L. H. Coudert, O. Pirali, M. Vervloet, R. Lanquetin, and C. Camy-Peyret, J. Mol. Spectrosc. **228**, 471 (2004).
[180]J. Kauppinen, T. Kärkkäinen, and E. Kyrö, J. Mol. Spectrosc. **71**, 15 (1978).
[181]J.-Y. Mandin, J.-P. Chevillard, C. Camy-Peyret, and J.-M. Flaud, J. Mol. Spectrosc. **118**, 96 (1986).
[182]M. P. Esplin, R. B. Wattson, M. L. Hoke, and L. S. Rothman, J. Quant. Spectrosc. Radiat. Transfer **60**, 711 (1998).
[183]R. A. Toth, J. Mol. Spectrosc. **190**, 379 (1998).
[184]A. Valentin, C. Claveau, A. D. Bykov, N. N. Lavrentieva, V. N. Saveliev, and L. N. Sinitsa, J. Mol. Spectrosc. **198**, 218 (1999).
[185]N. F. Zobov, O. L. Polyansky, J. Tennyson, J. A. Lotoski, P. Colarusso, K.-Q. Zhang, and P. F. Bernath, J. Mol. Spectrosc. **193**, 118 (1999).
[186]S. N. Mikhailenko, V. G. Tyuterev, V. I. Starikov, K. K. Albert, B. P. Winnewisser, M. Winnewisser, G. Mellau, C. Camy-Peyret, R. Lanquetin, J.-M. Flaud, and J. W. Brault, J. Mol. Spectrosc. **213**, 91 (2002).
[187]K. Tereszchuk, P. F. Bernath, N. F. Zobov, S. V. Shirin, O. L. Polyansky, N. I. Libeskind, J. Tennyson, and L. Wallace, Astrophys. J. **577**, 496 (2002).
[188]R. N. Tolchenov and J. Tennyson, J. Mol. Spectrosc. **231**, 23 (2005).
[189]R. Tolchenov and J. Tennyson, J. Quant. Spectrosc. Radiat. Transfer **109**, 559 (2008).
[190]A. Liu, O. Naumenko, S. Kassi, and A. Campargue, J. Quant. Spectrosc. Radiat. Transfer **110**, 1781 (2009).
[191]L. R. Brown and C. Plymate, J. Mol. Spectrosc. **199**, 166 (2000).
[192]O. L. Polyansky, N. F. Zobov, S. Viti, J. Tennyson, P. F. Bernath, and L. Wallace, J. Mol. Spectrosc. **186**, 422 (1997).
[193]O. L. Polyansky, N. F. Zobov, S. Viti, and J. Tennyson, J. Mol. Spectrosc. **189**, 291 (1998).
[194]P. Macko, D. Romanini, S. N. Mikhailenko, O. V. Naumenko, S. Kassi, A. Jenouvrier, V. G. Tyuterev, and A. Campargue, J. Mol. Spectrosc. **227**, 90 (2004).
[195]D. Lisak and J. T. Hodges, J. Mol. Spectrosc. **249**, 6 (2008).
[196]R. N. Tolchenov, J. Tennyson, J. W. Brault, A. A. D. Canas, and R. Schermaul, J. Mol. Spectrosc. **215**, 269 (2002).
[197]L. R. Brown, R. A. Toth, and M. Dulick, J. Mol. Spectrosc. **212**, 57 (2002).
[198]P.-F. Coheur, P. F. Bernath, M. Carleer, R. Colin, O. L. Polyansky, N. F. Zobov, S. V. Shirin, R. J. Barber, and J. Tennyson, J. Chem. Phys. **122**, 074307 (2005).
[199]R. N. Tennyson, O. Naumenko, N. F. Zobov, S. V. Shirin, O. L. Polyansky, J. Tennyson, M. Carleer, P.-F. Coheur, S. Fally, A. Jenouvrier, and A. C. Vandaele, J. Mol. Spectrosc. **233**, 68 (2005).

[200]J.-P. Chevillard, J.-Y. Mandin, J.-M. Flaud, and C. Camy-Peyret, Can. J. Phys. **67**, 1065 (1989).
[201]M. Carleer, A. Jenouvrier, A.-C. Vandaele, P. F. Bernath, M. F. Mérienne, R. Colin, N. F. Zobov, O. L. Polyansky, J. Tennyson, and V. A. Savin, J. Chem. Phys. **111**, 2444 (1999).
[202]N. F. Zobov, D. Belmiloud, O. L. Polyansky, J. Tennyson, S. V. Shirin, M. Carleer, A. Jenouvrier, A.-C. Vandaele, P. F. Bernath, M. F. Mérienne, and R. Colin, J. Chem. Phys. **113**, 1546 (2000).
[203]P. Dupré, T. Gherman, N. F. Zobov, R. N. Tolchenov, and J. Tennyson, J. Chem. Phys. **123**, 154307 (2005).
[204]F. Mazzotti, O. V. Naumenko, S. Kassi, A. D. Bykov, and A. Campargue, J. Mol. Spectrosc. **239**, 174 (2006).
[205]A. Campargue, S. Mikhailenko, and A. W. Liu, J. Quant. Spectrosc. Radiat. Transfer **109**, 2832 (2008).
[206]L. A. Pugh and K. Narahari Rao, J. Mol. Spectrosc. **47**, 403 (1973).
[207]J.-M. Flaud, C. Camy-Peyret, J.-P. Maillard, and G. Guelachvili, J. Mol. Spectrosc. **65**, 219 (1977).
[208]J.-M. Flaud, C. Camy-Peyret, K. Narahari Rao, D.-W. Chen, and Y.-S. Hoh, J. Mol. Spectrosc. **75**, 339 (1979).
[209]C. Camy-Peyret, J. M. Flaud, and J.-P. Maillard, J. Phys. Lett. **41**, L23 (1980).
[210]C. Camy-Peyret, J.-M. Flaud, J.-Y. Mandin, J.-P. Chevillard, J. Brault, D. A. Ramsay, M. Vervloet, and J. Chauville, J. Mol. Spectrosc. **113**, 208 (1985).
[211]J.-Y. Mandin, J.-P. Chevillard, J.-M. Flaud, and C. Camy-Peyret, Can. J. Phys. **66**, 997 (1988).
[212]V. Dana, J.-Y. Mandin, C. Camy-Peyret, J.-M. Flaud, and L. S. Rothman, Appl. Opt. **31**, 1179 (1992).
[213]V. Dana, J.-Y. Mandin, C. Camy-Peyret, J.-M. Flaud, J.-P. Chevillard, R. L. Hawkins, and J.-L. Delfau, Appl. Opt. **31**, 1928 (1992).
[214]J.-Y. Mandin, V. Dana, C. Camy-Peyret, and J.-M. Flaud, J. Mol. Spectrosc. **152**, 179 (1992).
[215]O. L. Polyansky, J. R. Busler, B. Guo, K. Zhang, and P. F. Bernath, J. Mol. Spectrosc. **176**, 305 (1996).
[216]O. L. Polyansky, J. Tennyson, and P. F. Bernath, J. Mol. Spectrosc. **186**, 213 (1997).
[217]A. Bykov, O. Naumenko, L. Sinitsa, B. Voronin, J.-M. Flaud, C. Camy-Peyret, and R. Lanquetin, J. Mol. Spectrosc. **205**, 1 (2001).
[218]O. Naumenko and A. Campargue, J. Mol. Spectrosc. **221**, 221 (2003).
[219]S. Kassi, P. Macko, O. Naumenko, and A. Campargue, Phys. Chem. Chem. Phys. **7**, 2460 (2005).
[220]T. Petrova, Y. Poplavskii, V. Serdukov, and L. Sinitsa, Mol. Phys. **104**, 2691 (2006).
[221]N. F. Zobov, S. V. Shirin, O. L. Polyansky, R. J. Barber, J. Tennyson, P.-F. Coheur, P. F. Bernath, M. Carleer, and R. Colin, J. Mol. Spectrosc. **237**, 115 (2006).
[222]O. V. Boyarkin and N. F. Zobov (private communication, 2012).
[223]R. A. Toth and J. S. Margolis, J. Mol. Spectrosc. **55**, 229 (1975).
[224]O. L. Polyansky, N. F. Zobov, J. Tennyson, J. A. Lotoski, and P. F. Bernath, J. Mol. Spectrosc. **184**, 35 (1997).
[225]S. Béguier, S. Mikhailenko, and A. Campargue, J. Mol. Spectrosc. **265**, 106 (2011).
[226]J.-M. Flaud, C. Camy-Peyret, A. Bykov, O. Naumenko, T. Petrova, A. Scherbakov, and L. Sinitsa, J. Mol. Spectrosc. **183**, 300 (1997).
[227]R. Lanquetin, L. H. Coudert, and C. Camy-Peyret, J. Mol. Spectrosc. **206**, 54 (2001).
[228]See https://spec.jpl.nasa.gov//ftp//pub/catalog/archive/c018005.egy for JPL website, 2005; accessed 16 March 2020.
[229]H. M. Pickett, J. C. Pearson, and C. E. Miller, J. Mol. Spectrosc. **233**, 174 (2005).
[230]National Academies of Sciences, Engineering, and Medicine, *Frequency Allocations and Spectrum Protection for Scientific Uses*, 2nd ed. (The National Academies Press, Washington D.C., 2015).
[231]S. N. Mikhailenko, S. Kassi, D. Mondelain, and A. Campargue, J. Quant. Spectrosc. Radiat. Transfer **245**, 106840 (2020).